AFOSR TR-97-0430

REPORT DOCUMENTATION PAGE

Form Approved
OMB No. 0704-0188

1. AGENCY USE ONLY (Leave blank)	2. REPORT DATE	3. REPORT TYPE AND DATES COVERED
	August 28, 1997	Final Tech. Report 4/1/93-3/31/97

4. TITLE AND SUBTITLE
Thermal Relaxation Processes and Stability in Poled Electro-Optic Polymers

5. FUNDING NUMBERS
G
F49620-93-1-0202
PR/TA
2303/CS
61102F

6. AUTHOR(S)
Kenneth D. Singer

7. PERFORMING ORGANIZATION NAME(S) AND ADDRESS(ES)
Case Western Reserve University
10900 Euclid Ave
Cleveland, OH 44106-7015

8. PERFORMING ORGANIZATION REPORT NUMBER
342-4775

9. SPONSORING/MONITORING AGENCY NAME(S) AND ADDRESS(ES)
AFOSR/~~NC~~NL
110 Duncan Ave, Suite B115
Bolling AFB, DC 20332-0001
Dr Lee

10. SPONSORING/MONITORING AGENCY REPORT NUMBER

11. SUPPLEMENTARY NOTES

12a. DISTRIBUTION/AVAILABILITY STATEMENT
Approved for public release;
distribution unlimited.

12b. DISTRIBUTION CODE

13. ABSTRACT *(Maximum 200 words)*

The goal of gaining better understanding of the orientational decay mechanisms of poled nonlinear optical polymers and to develop a predictive description of the long time scale decay was well met. We developed a new experimental technique based on electric field induced second harmonic generation in the frequency domain to probe the polymer over many decades of time. This technique is best applied near the glass transition to probe frequencies from mHz to tens of kHz. We used this technique along with others to study a variety of polymers. Applying an Adams-Gibb model to the temperature dependence of the characteristic frequency, prediction of long term behavior at any temperature based on quick measurements near the glass transition temperature is possible. We also developed a new ultrafast laser source for studying nonlinear optical susceptibilities, and contributed to the study of cross-linked polyimide materials as stable and processable hosts for poled electro-optic polymers.

14. SUBJECT TERMS	15. NUMBER OF PAGES
Nonlinear and Electro-Optic Polymers	76
	16. PRICE CODE

17. SECURITY CLASSIFICATION OF REPORT	18. SECURITY CLASSIFICATION OF THIS PAGE	19. SECURITY CLASSIFICATION OF ABSTRACT	20. LIMITATION OF ABSTRACT
Unclassified			UL

NSN 7540-01-280-5500

Standard Form 298 (Rev. 2-89)
Prescribed by ANSI Std. Z39-18
298-102

Summary of Results and Accomplishments

Technical summary

Electro-optic polymer relaxation

Objective:

To better understand the orientational decay mechanisms of poled second-order NLO polymers and to develop a predictive description of the long time scale (in terms of tens of years) orientational decay of poled polymer systems.

Approach:

An electric field poling process is used to create noncentrosymmetric order in polymer hosts containing dipolar nonlinear optical chromophores. The resulting materials have been found useful for producing a variety of nonlinear optical and electro-optic devices. The easy processability into thin films make such material ideal for waveguide electro-optic devices. A number of companies are now developing such commercial devices.

A major issue in these materials arises from the nonequilibrium nature of the polymers resulting in the eventual decay of the nonlinear optical response, which is due to the reorientation of the aligned chromophores into a randomly oriented state. Therefore, much research has centered on understanding the decay mechanism with the goal to guide the design of new and more stable materials. To this end, our program aims to develop a predictive model, which is tied to relevant material parameters such as the glass transition temperature, and the relaxation behavior at this temperature. As materials improve, and stability increases, the need for accelerated testing increases. Thus, we seek to develop models and measurement regimes that probe behavior at high temperatures (thus short times) and can be connected theoretically to low temperature (thus long time) behavior.

The orientational relaxation of nonlinear optical chromophores, which are aligned within a polymer using electric field poling techniques, is highly coupled to the relaxation behavior of the host polymer glass. Polymer glasses are well known to display highly dispersive relaxation behavior as the glass tends toward equilibrium. This dispersive behavior is manifested in relaxation processes being spread over all time scales. Indeed, it is believed that such behavior is self-similar over a very wide-range of time scales. Additionally, it has been found that time and temperature behavior can be superimposed. We wanted to develop measurement techniques that probe the relaxing nonlinear optical chromophore directly, and to be able to probe the coupling to the polymer over as wide a time and temperature scale as possible. By doing this, we could relate the chromophore relaxation to the dielectric relaxation in the polymer. The concept of superposition of time and temperature will allow for the development of accelerated lifetime testing when an appropriate model is developed.

We studied the relaxation behavior over many decades of time using frequency and time domain techniques. Based on these results, we were better able to probe a wide temperature range to ascertain the characteristic times and dispersion parameters of the relaxation phenomena. We were then able to determine which models best fit the data, and then to use these models to predict behavior at different temperatures and time scales.

Results:

We have assembled the temperature control system shown in Figure 1 which can access temperature from liquid nitrogen temperature to about 150 C. We have a separate cell which can access temperatures to 300 C. The apparatus in Figure 1 consists of a liquid nitrogen dewar with a resistance heater which is temperature controlled. This system has been built to be capable of carrying out electrical measurements concurrent with the nonlinear optical measurements. Thus, we have the capability to measure the dielectric constant, resistivity, thermally stimulated depolarization, and isothermal depolarization. These measurements will be able to characterize the relaxation behavior of the polymer over an extremely wide range of times so as to best determine the appropriate model (see above) which describes the relaxation.

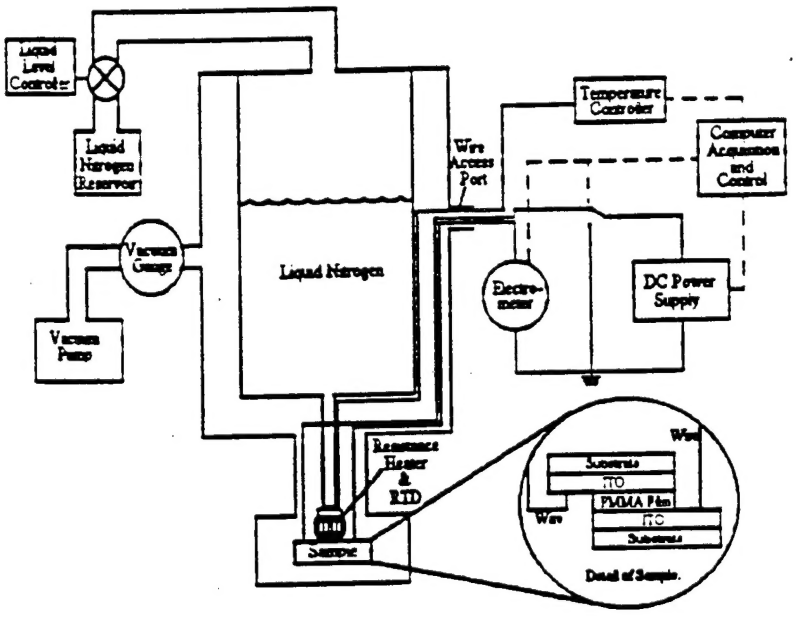

Figure 1. Dewar system.

We built a chielectric spectroscopy apparatus for measuring the orientation response of the nonlinear optical chromophore directly in the frequency domain. This is a new technique, which we have improved by using a mode-locked CW laser and a lock-in amplifier to measure the frequency response of electric field induced second harmonic generation over a broad frequency range. The mode-locked Ti:Sapphire laser is described Richard Dureiko's Ph.D. Thesis. The experimental setup is shown if Figure 2. The entire chielectric experiment is described in detail in Appendix 1. This technique was found useful for measurements near and above the glass transition temperature.

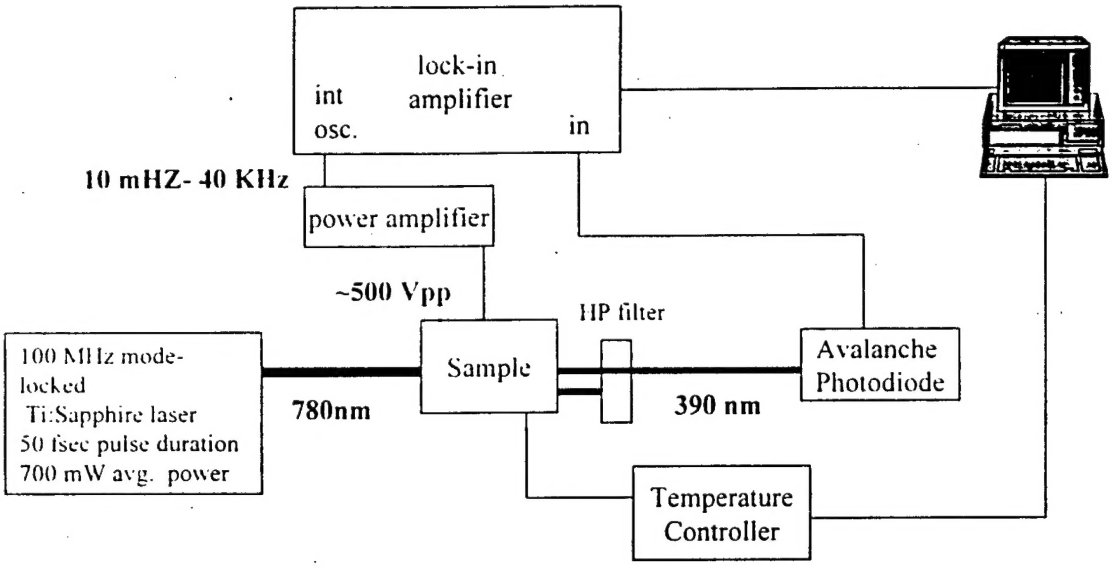

Figure 2. Chielectric spectroscopy setup.

We measured the dielectric and chielectric response near and above the glass transition in the frequency domain for a series of doped and covalent polymers based on methyl methacrylate and in cross-linked materials provided by L. Dalton (see R. Dureiko thesis). We also measured the dielectric and chielectric response in the time domain below the glass transition temperature. Using all four techniques, we were able to probe the response on many time scales and temperature regimes.

We analyzed the isothermal data in terms of a three parameter relaxation model as adapted from the model of Dissado and Hill. This analysis provides the dispersion parameters and characteristic times of the relaxation. The data was collected at a range of temperatures both above and below the glass transition temperature, and from it we could conclude that a three-parameter model including dispersion and asymmetry was

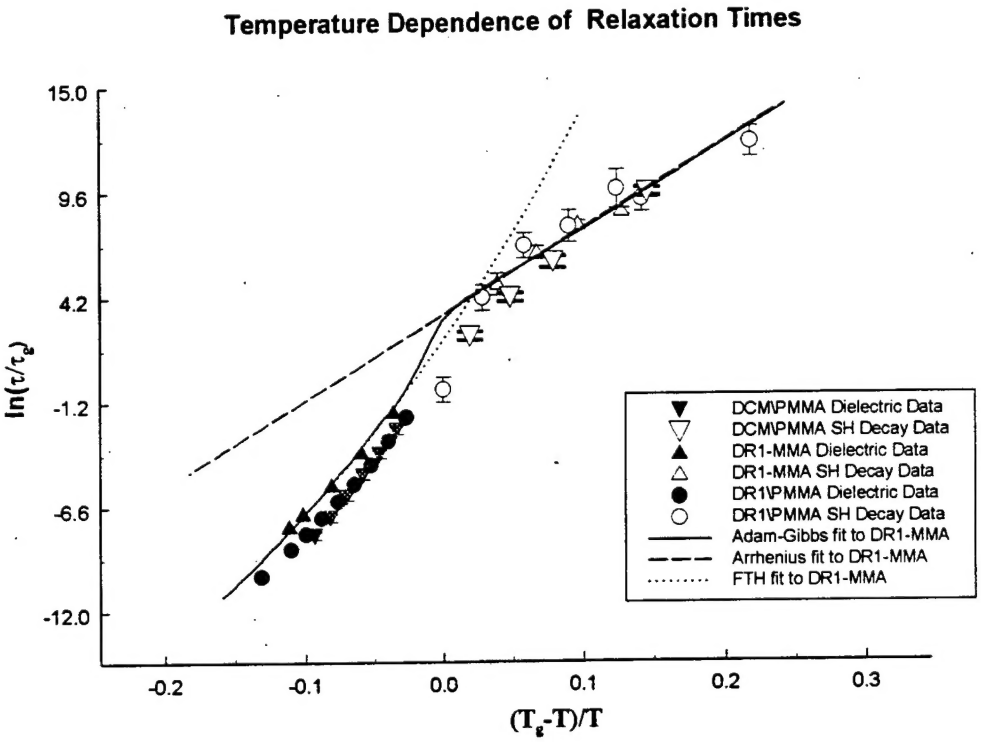

Figure 3. Reduced temperature dependence plot for τ scaled to τ_g for the three polymer systems. The solid line represents the Adam-Gibbs model based on enthalpy measurements from DR1-MMA. The dashed line represents an Arrhenius fit based on data points below the glass transition, while the dotted line represents Fulcher-Tammann-Hesse or equivalently WLF behavior above the glass transition.

necessary to fit the data. A single constant diffusive model and even the widely used KWW function was inadequate to fit the data over the many time decades we were able to measure. Thus our program of time and frequency domain measurements scanning many decades of time was able to differentiate between models for the isothermal relaxation.

Finally, we applied the Adam-Gibbs model to the isothermal data at many temperatures. Again, our technique provided for measurement over many time scales which also allows determination of the characteristic times over a wide temperature range. This allowed for good comparison to the Adam-Gibbs model. In this model, the temperature behavior is well-described both above and below the glass transition. The model agrees with other models which are only applicable over limited temperature ranges. Thus, the model is

able to connect high temperature (short time) measurements with low temperature (long time) measurements and provides the basis for a predictive model. In addition, the characteristic times were normalized to that at the glass transition and the temperature to the glass transition in a data plot as shown in Figure 3. Using this technique, predictive capability results, and further, it is seen that similar polymers fall onto a single curve for quasi-universal behavior. Thus predictions can be made on closely related systems using the glass transition as a scaling parameter. This allows for guidance in new material development. Details in Appendix 1.

We believe that we have attained the major goals of the program. We have identified a model and measurement regime appropriate for accelerated failure tests, which can aid in the development of more stable electro-optic polymers. In doing this, we have developed a new measurement technique, chielectric spectroscopy, which can be applied to study basic questions in polymer physics. Since the technique is sensitive only to the chromophores, it can be used to study whether the relaxation is a collective effect of the dipoles.

Laser system development

We built a new tunable laser source for harmonic generation experiment. The system consists of an active-passive modelocked Nd:YAG laser with negative feedback in the oscillator to produce a train of about 50 20 picosecond pulses during each lampflash. The laser contains a double pass amplifier followed by frequency tripling crystals whose output pumps a parametric oscillator. It is the first subpicosecond Nd:YAG based laser source. It uses a synchronously pumped optical parametric oscillator (SPOPO) which when properly tuned generates subpicosecond tunable laser light. Pulses as short as 400 fs have been observed. The system uses BBO crystals and is tunable from 450-2500 nm.

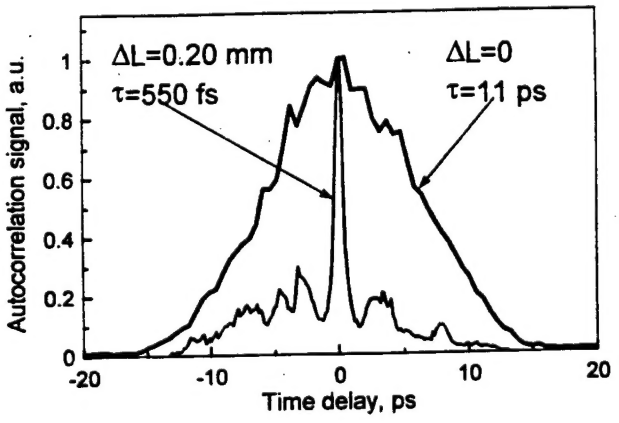

Figure 4. Autocorrelation trace of subpicosecond laser pulses from the SPOPO depicting pulse compression.

Short pulses are generated using group velocity walk off in the slightly detuned SPOPO. We have modeled the pulse generation mechanism using the coupled wave equations in the nonlinear optical crystal and have studied the mechanism responsible. The pulse compression involves the group velocity walk off and the depleted parametric conversion. It is believed that the compressed pulses are 3 wave temporal solitons.

This unique source was utilized to measure the dispersion in third harmonic generation in squaraine dyes. In addition, we have recently used this laser as the core of the only widely tunable hyper-Rayleigh scattering apparatus. We have used it to study the dispersion of hyper-Rayleigh scattering, and have identified dephasing as a problem in the measurement of near-resonant hyper-Rayleigh scattering. Most recently, we have measured Kleinman-symmetry-breaking in organic molecules, which are candidates for a new class of "quadrupoled" polymeric materials.

Crosslinked polyimide materials for integrated optics

We have been studying a promising new class of materials based on crosslinkable polymers developed by Amoco Chemical Co. The crosslinking makes the materials desirable for stable electro-optic films, and their photosensitivity makes device processing extremely attractive.

We studied the structure property relationships associated with waveguide losses and successfully developed very low loss materials which are now being investigated by a number of companies for waveguide passive interconnect applications. We have successfully poled nonlinear optical molecules in these polymers and have observed stable electro-optic properties.

We have investigated poling through multilayer waveguide structures and have developed a technique to dope the cladding, which concentrates the poling field in the active layer. This approach led to nearly a tenfold increase in electro-optic coefficient.

Devices in similar materials are now under development by Lockheed-Martin. Details are given in Appendix 2.

Personnel Supported

Richard Dureiko, Ph.D. student
Thesis: Relaxation Processes in Poled Electro-Optic Polymer Films
Passed Ph.D. Exam, Ph.D. Physics, degree to be awarded January, 1998
Currently employed at Corning Corp.

John D.V. Khaydarov, Research Associate (Postdoctoral)
Currently employed at Continuum Laser Co.

Anthony C. Kowalczyk, Ph.D. student
Thesis: Second Order Optical Nonlinearities in Polymeric Waveguides
Ph.D. Physics, degree awarded, January 1996
Currently employed at Deacon Research

Russell Fuerst, Undergraduate student
Degree: B.S. Physics, May, 1995
Currently Ph.D. student at Univ. Cent. Florida, CREOL

Andrew Schober, Undergraduate student
Degree: B.S. Physics, expected May, 1998

Lectures and Publications

Invited Lectures

1. K.D. Singer, T.C. Kowalczyk, H. Nguyen, A. Beuhler, and D. Wargowski, "Cross-Linked Polyimides for Integrated Optics", *Proc. SPIE* **CR68** (1997).

2. K.D. Singer, R.D. Dureiko, D.E. Schuele, "Chielectric Relaxation in Poled Electro-optic Polymer Films", *Proc. SPIE* **3147** (1997).

3. K.D. Singer and R.D. Dureiko, "Modeling Relaxation Mechanisms in Nonlinear Optical Polymer Systems", OSA/ACS Topical Meeting on Organic Thin Films for Photonics Applications, Long Beach, CA, October, 1997.

4. K.D. Singer, T.C. Kowalczyk, H. Nguyen, A. Beuhler, and D. Wargowski, "Cross-Linked Polyimides for Integrated Optics", Proc. SPIE 3006, 326 (1997).

5. K.D. Singer, J.H. Andrews, J.D.V. Khaydarov, "Generation of Compressed Pulses in a Synchronously Pumped Optical Parametric Oscillator", LASERS '94, Quebec, 1994.

6. K.D. Singer, "Polymeric Nonlinear Optical Materials", OSA/ACS Symposium on Polymeric Thin Films for Photonic Applications, Washingon, D.C., August 21-24, 1994.

7. K.D. Singer, "Orientational Relaxation Phenomena in Electro-optic Polymers", Gordon Research Conference on Dielectric Phenomena, Holderness School, NH July 31-August 5, 1994.

8. K.D. Singer, R. Dureiko, J. Khaydarov, and R. Fuerst, "Relaxation in Poled Electro-optic Polymers", 4th Iketani Conference, Hawaii, May 17-20, 1994.

9. J.H. Andrews, J.D.V. Khaydarov, and K.D. Singer, "Third Harmonic Dispersion Studies of a Squarate Dye: Probing the 2^1Ag State", ICONO'1, Val Thorens, France, January, 1994.

10. K.D. Singer, R. Dureiko, J. Khaydarov, and R. Fuerst, "Relaxation Phenomena in Poled Electro-Optic Polymers", *Proc. Mat. Res. Soc.* **328**, 499 (1994).

11. R.A. Fuerst, "Thermal Relaxation Processes and Stability in Poled Electro-optic Materials", Research Project Symposium Day, Ohio Space Grant Consortium, Ohio Aerospace Institute, Cleveland, OH.

Submitted Lectures

1. R.D. Dureiko, D.E. Schuele, and K.D. Singer, "Chielectric relaxation in poled electro-optic films", QELS, Baltimore, MD. May, 1997.

2. R.D. Dureiko and K.D. Singer, "Modeling Relaxation Processes in Poled Electro-optic Polymers", Third International Conference on Organic Nonlinear Optics (ICONO'3), Marco Island, FL, December 16-20, 1996.

3. J.D. Khaydarov, J.H. Andrews, K.D. Singer, "Soliton-like compressed pulses in a synchronously pumped optical parametric oscillator", Optical Society of America, Rochester, NY, October, 1996.

4. K.D. Singer, J.H. Andrews, J.D.V. Khaydarov, D.L. Hull, and K.C. Chuang, "Contributions of Low-Lying Excited States to Optical Nonlinearities in Squaraines" Materials Research Society, Boston, MA December, 1995.

5. J.H. Andrews, J.D.V. Khaydarov, K.D. Singer, D.L. Hull, K.C. Chuang, "Third Harmonic Dispersion Studies of Centrosymmetric and Noncentrosymmetric Squaraines", ACS/OSA Topical Meeting: Organic Thin Films for Photonics Applications, Portland, OR, Sept. 11-14, 1995.

6. T.C. Kowalczyk, T.Z. Kosc, K.D. Singer, A.J. Beuhler, D.A. Wargowski, P.A. Cahill, C.H. Seager, and M.B. Meinhardt, "Guest-Host Crosslinked Polyimides for Integrated Optics", ACS/OSA Topical Meeting: Organic Thin Films for Photonics Applications, Portland, OR, Sept. 11-14, 1995.

7. K.D. Singer, J.H. Andrews, and J.D.V. Khaydarov, "Pulse Compression in a Synchronously Pumped Optical Parametric Oscillator", CLEO, Baltimore, Md., May 21-26, 1995.

8. J.H. Andrews, J.D.V. Khaydarov, K.D. Singer, D. Hull, and K. Chuang, "Third Harmonic Spectral Dispersion of Squaraines", Symposium on Polymeric Thin Films for Photonic Applications, ACS Annual Meeting, Washington, DC, August 21-24, 1994.

9. K.D. Singer, T.C. Kowalczyk, T.Z. Kosc, A.J. Buehler, D.A. Wargowski, P.A. Cahill, C.H. Seager, M.G. Meinhardt, and S. Ermer, "Polymer Electro-optic Materials", Electronic Materials Conference, Boulder, CO., June 22-24, 1994.

10. J.D.V. Khaydarov, J.H. Andrews, and K.D. Singer, "Dispersive Pulse Compression in a Synchronously Pumped Optical Parametric Oscillator", CLEO, Anaheim, CA. May 8-13, 1994.

11. J.H Andrews, J.D.V. Khaydarov, and K.D. Singer, "Third-harmonic Dispersion Studies of a Squarate Dye: Probing the 2^1Ag State", IQEC, Anaheim, CA. May 8-13, 1994.

Journal Publications

1. R.D. Dureiko, D.E. Schuele, and K.D. Singer, "Modeling Relaxation Processes in Poled Electro-Optic Polymer Films", *J. Opt. Soc. Am. B* January, 1998.

2. A.J. Beuhler, D.A. Wargowski, K.D. Singer, and T. Kowalczyk, "Fabrication of Low Loss Polyimide Optical Waveguides Using Thin-Film Multichip Module Process Technology", *IEEE Trans. Comp., Pack., and Manuf. Tech. B* **18**, 232 (1995).

3. J.H. Andrews, J.D.V. Khaydarov, K.D. Singer, D.L. Hull, K.C. Chuang, "Characterization of Excited States of Centrosymmetric and Noncentrosymmetric Squaraines by Third Harmonic Spectral Dispersion", *J. Opt. Soc. Am. B* **12**, 2360 (1995).

4. T.C. Kowalczyk, T.Z. Kosc, K.D. Singer, A.J. Beuhler, D.A. Wargowski, P.A. Cahill, C.H. Seager, and M.B. Meinhardt, "Crosslinked Polyimide Electro-optic Materials", *J. Appl. Phys.* **78**, 5876 (1995).

5. J.D.V. Khaydarov, J.H. Andrews, and K.D. Singer, "Pulse Compression Mechanism in a Synchronously Pumped Optical Parametric Oscillator", *J. Opt. Soc. Am. B* **12**, 2199 (1995).

6. J.D.V. Khaydarov, J.H. Andrews, and K.D. Singer, "20-Fold Pulse Compression in a Synchronously Pumped Optical Parametric Oscillator", *Appl. Phys. Lett.* **65**, 1614 (1994).

7. J.H. Andrews, J.D.V. Khaydarov, K.D. Singer, D.L. Hull, and K.C. Chuang, "Spectral Dispersion of Third Harmonic Generation in Squaraines", *Nonlinear Optics*, **10**, 227 (1995)

8. J.H. Andrews, J.D.V. Khaydarov, and K.D. Singer, "Contribution of the 2^1Ag State to the Third Order Optical Nonlinearity in a Squaraine Dye", *Opt. Lett.*, **19**, 984 (1994).

9. J.D.V.Khaydarov, J.H. Andrews, and K.D. Singer, "Pulse Compression in a Synchronously Pumped Optical Parametric Oscillator Due To Group Velocity Mismatch", *Opt. Lett.* **19**, 831 (1994).

10. K.D. Singer and J.H. Andrews, "Origin of Third-order Optical Nonlinearities in Centrosymmetric Organic Materials", *Condensed Matter News* **3**, 7 (1994).

11. J.D.V. Khaydarov, J.H. Andrews, and K.D. Singer, "20-Fold Pulse Compression in a Synchronously Pumped Optical Parametric Oscillator", *Appl. Phys. Lett.* **65**, 1614 (1994).

Appendix 1

Modeling Relaxation Processes in Poled Electro-Optic Polymer Films
R. D. Dureiko, D.E. Schuele, and K.D. Singer

J. Opt. Soc. Am. B (In Press, to appear January, 1998)

Modeling Relaxation Processes in Poled Electro-Optic Polymer Films

R.D. Dureiko, D.E.Schuele, and K.D. Singer
Case Western Reserve University
Department of Physics
Cleveland, Ohio 44106-7079

Abstract

Chielectric spectroscopy, which is frequency domain electric field induced second harmonic generation, was developed to study the nonlinear optical response near the glass transition temperature at short time scales. These measurements, along with time domain second harmonic generation and time and frequency domain dielectric measurements were used to characterize the decay of poling-induced electro-optic properties of guest-host and side-chain methacrylate polymers having glass transition temperatures in the range of $90< T_g <125$ °C. Time and frequency dependent data were modeled with the model of Dissado and Hill. The temperature dependence of the time constants from the polymeric systems were then compared and a scaling model for predicting useful lifetimes of poled electro-optic media is discussed.

1. Introduction

Over the past decade, a great deal of research has been focused on the development of nonlinear optical (NLO) and electro-optic (EO) polymeric materials because of their potential in applications ranging from second harmonic generation (SHG) and phase conjugation, to optical switching and electro-optic modulation.[1,2,3] Due to their large nonlinear optical properties, ease of processing, and expected low cost, polymers are leading candidates for electro-optic materials.

Electric-field poling has become a favored technique for producing noncentrosymmetric polymeric electro-optic materials. Here, nonlinear optical molecules incorporated in a polymer host are aligned in an electric field when in a highly mobile state, and the resulting polar orientational order is "locked-in" by cooling or chemical reaction. The decay of the electro-optic and nonlinear optical properties arises from the relaxation of the polar orientational alignment originally induced in the electric field poling process. The polar orientational order eventually reverts to the original isotropic alignment present prior to poling, and is due to the orientational mobility of the aligned nonlinear optical chromophores as well as to the relaxational motion of the polymer host in its non-equilibrium state. In order for a polymeric device to be viable, it must retain its NLO properties over the course of the required lifetime of the device, which may be several years. The usefulness of devices based on these poled polymeric materials is dependent upon the temporal and temperature stability of the NLO properties of the material.

Since the earliest poling experiments, the instability of the orientational order was recognized, as were paths to the development of new materials which would enhance the stability.[4,5] A great deal of effort has gone into developing new stable materials as well as into studies aimed at understanding the process underlying the relaxation. It has been found that a close relationship exists between the decay of the electro-optic coefficient and other relaxation processes in polymers, and so has been able to draw on that literature. A number of approaches have been taken to describe the process, and great progress has been made in developing a predictive model for the lifetime of electro-optic polymers.[1]

In this paper, our aim is to move closer to a universal predictive model and a regime of measurements useful in predicting lifetime from measurements taken in a short time. We have approached the subject with the goal of unifying the disparate approaches that have been used in the past by seeking models for the

process which subsume previously published models. We begin with a review of the literature in the context of models and experimental techniques and then describe these in relation to the somewhat more general models we propose here. In addition, we describe a recently developed experimental technique, "chielectric spectroscopy", which measures electric field induced second harmonic generation in the frequency (modulating) domain. This technique is analogous to dielectric spectroscopy except that it directly probes only the nonlinear optical chromophore. With this technique and time-domain second harmonic generation decay measurements, a wide frequency range of the orientational response can be probed, corresponding to a wide range of temperatures and times. Finally, we describe measurements on acrylate polymers in the context of our proposed experimental regime and models with the goal of a predictive model.

2. Orientation Relaxation Models

As mentioned previously, a requirement for second-order nonlinear and Pockels materials is that the material lacks an inversion center (noncentrosymmetric). The electric field poling process has been developed to impose this symmetry on otherwise isotropic polymer materials containing nonlinear optical chromophores. In this process, polar order is imposed which can be described by an oriented gas model, for which the Pockels coefficient is given by,[5]

$$r_{ii}(-\omega;\omega,0) = N\left\langle \cos^3\theta \right\rangle f^{\omega} f^{\omega} f^{0} \beta_{zzz}(-\omega;\omega,0) \qquad (1)$$

where N is the number density of nonlinear optical chromophores, the f's are local field factors at the specified frequencies, $\beta_{zzz}(-\omega;\omega,0)$ is the molecular hyperpolarizability, and $\langle\cos^3\theta\rangle$ is a thermal average which depends on the angle between the molecular dipole and the poling field direction, the strength of the molecular dipole moment, μ, and the strength of the applied field, E. This thermal average is the order parameter, and decays with time due to the orientational mobility of the chromophore and the relaxational motion of the polymer host. Once the field is removed, the chromophores find themselves in a thermal non-equilibrium environment, and will tend to randomly orient themselves with respect to each other,

resulting in a decay of r_{33} over time.[6,7] This relaxation of the chromophore dipoles is hindered by the polymer matrix which surrounds them.

When the poling field is turned off, one can detect the orientational relaxation through a measurement of the second harmonic or electro-optic coefficient. A description of the decay of the optical nonlinearity has two parts which ultimately provide for the time and temperature dependence of the decay of the nonlinear optical properties. In the first part, the time dependence of the isothermal decay is modeled using chromophore reorientation models, a number of which are described below. These models require experimentally determined parameters which characterize the decay function. In polymer systems, two or three parameters should suffice, although some models contain more. Generally, one of the parameters describes the characteristic time of the system, while the other one or two parameters describe the dispersive nature of the decay exhibited in viscoelastic systems like polymers. These parameters are characteristic of the materials and the processing history. It is well known from the dielectric literature, that the time dependence can be probed in the frequency domain. We further develop this approach here with the measurement of chielectric spectroscopy where frequency dependent electric field induced second harmonic generation is studied. Measurements in the time and frequency domains are equivalent and are related through appropriate mathematical transforms. In the second part of developing a model, a physical picture of the material properties contributing to the decay is drawn. This part, the relaxation model, will describe the temperature dependence of the parameters describing the chromophore reorientation which are obtained through a fit to the isothermal time-dependent data. Here the statistical physics is introduced and related to the temperature dependence of the chromophore reorientation parameters. We will now review the models used in the literature and introduce our models of choice here, namely the Dissado-Hill model for the chromophore reorientation, and the Adams-Gibbs model of the relaxation.

2.1. Chromophore reorientation

2.1.1. Previously studied models

One of the simplest decay models is the Debye model.[8] In this model, chromophore orientational relaxation is described by a single exponential function,

$$P(t) = P_0 \exp(-t/\tau) \tag{2}$$

where P represents the nonlinear optical polarization and τ is a characteristic relaxation time. Thus, the square root of the second harmonic intensity versus time could be fit to this function where applicable. This one parameter model is helpful in describing relaxation in gases and dilute low viscosity liquids. The shortfall of this simple model is borne out in experimental data that clearly indicates that it fails to describe the time dependence of the orientational decay in viscoelastic materials, as has been pointed out by a number of workers.[9,10,11,12] The Debye model fails to capture the dispersive nature of the relaxation in such materials. The failure of this model can be understood, for example, by considering that the individual chromophores undergoing reorientation are surrounded by a complex polymer network that hinders their rotations. Due to this network, individual chromophores will experience different molecular environments that hinder their relaxation, which means that one should expect a range of characteristic relaxation time constants instead of just one.

A second model addresses this aspect by taking into account that more than one characteristic time constant is needed to describe the orientational relaxation of the chromophore molecules in the polymer matrix. Thus, the distribution of relaxation times (DRT) improves upon the simple Debye model.[13, 14, 15, 16, 17, 18] This model is similar to the Debye model in that it assumes the relaxing dye molecules are completely independent of each other, and thus, there are no dipole-dipole interactions. It differs in that the nonlinear optical polarization is now written as a superposition of Debye relaxations.

$$P(t) = \sum_{i=0}^{\infty} P_i \exp(-t/\tau_i) \tag{3}$$

where the τ_i's represent the individual characteristic relaxation times. This can also be written for a continuous distribution described by a function $\rho(\tau)$ using,

$$P(t) = \int_0^{\infty} \rho(\tau)\exp(-t/\tau)d\tau \ . \tag{4}$$

Another model, which can be viewed as a limiting form of the discrete DRT model, is the bi-exponential model which describes the decay process in terms of only two characteristic time constants, τ_1, and τ_2,[19,20]

$$P(t) = P_1 \exp(-t/\tau_1) + P_2 \exp(-t/\tau_2) \tag{5}$$

Researchers, such as Goodson *et al.*[21] and Hampsch *et al.*[22] have found this type of model fits their second harmonic (SH) decay data well in PMMA polymer systems doped with DANS.

Currently, the most widely used empirical decay model in the literature is the Kohlrausch-Williams-Watts (KWW) or 'stretched exponential' model.

$$P(t) = P_0 \exp\left[-(t/\tau)^{\beta}\right] \tag{6}$$

where τ is the characteristic relaxation time constant and β is a parameter that varies between zero and unity. This model was introduced by Kohlrausch in 1847 to describe mechanical creep in glassy fibers[23] and then again over 100 years later in 1970 by Williams and Watts[24] to describe dielectric relaxation. Since then, this model has been used by several researchers to interpret SH decay data. [22,25,26,27] Although originally applied as an empirical law, researchers such as Klafter and Shlesinger,[28] and even more recently Weron[29] have tried to bring some physical meaning to this law. The KWW model can be related to the DRT model in that we can write it as,

$$\exp(-t/\tau)^{\beta} = \int_0^{\infty} \exp(-t/\tau)\, \rho(\tau)\, d\tau \tag{7}$$

where $\rho(\tau)$ is the distribution of Debye relaxation times introduced above.[30] In this interpretation, β is a shape parameter of the distribution function. When β is unity, the KWW function reduces to the Debye model. Several researchers have found that β increases with increasing temperature, but no good model of its temperature dependence exists.[26, 31]

The time scales over which experiments have monitored chromophore reorientation range from microseconds in DR1 doped PS[32] all the way out to a year in a polyimide side-chain polymer,[33] and in both studies, the KWW was used to fit the SH decay data.

Another empirical model put forth by Van der Vorst *et al.*[20] is a modified version of the classical Debye model. In this model the characteristic relaxation time constant now becomes a function of time,

$$P(t) = P_0 \exp(-t/\tau(t)), \qquad \tau(t) = \tau_0 + A\, t^{B} \tag{8}$$

where A, B and τ_0 are fit parameters. Adding these additional parameters to the model allowed a better fit to their experimental data on DANS side-chained polymers, however, the physical justification for doing so is unclear.

Several researchers have put forth relaxation models based on chromophore rotational Brownian motion in the polymer matrix.[34, 35] Liu et al.[36] have developed a Brownian motion model that also accounts for electric field effects, and polymer restrictions to describe their corona poled DANS doped PMMA systems. In their model,

$$\chi^{(2)}_{zzz} \approx N\, f_z(\omega)\, f_z(2\omega)\beta_{zzz} \int_0^{\theta_0} \cos^3\theta\; p(\theta,t;a,b,\theta_0,D)\sin\theta\, d\theta \qquad (9)$$

where f is the local field factor, N is the number of rotating chromophores, and β_{zzz} is the second- order polarizability of each chromophore. The effects due to the electric field are accounted for in the parameters a and b, and polymer restrictions are represented by the wedge angle θ_0. The only adjustable parameter in this model is the diffusion constant, D, the other parameters are determined in independent experiments. It has not been established that this model describes the dispersive nature of the relaxation.

As another example of the use of distributions of relaxation times (DRT) , Verbeist *et al.*[37] have shown that the Wagner or lognormal distribution function is useful in describing chromophore relaxation. In this model the decay function is described by a continuous distribution of exponential relaxation times,

$$P(t) = \frac{1}{\pi}\int_{-\infty}^{\infty} \exp\left(-u^2\right)\exp\left[-x\exp\left(-\beta_G u\right)\right]du \qquad (10)$$

where β_G is the half-width of the Gaussian distribution at the 1/e point, x is defined as τ/τ_m, with τ_m being the relaxation time associated with the maximum of the distribution function, and u defined as $\ln(\tau/\tau_m)$.

2.1.2. Dissado-Hill Many Body Model

Departing from the empirical models already reviewed above, we now briefly outline the Dissado-Hill (D-H) Many Body Universal Relaxation Model.[38] A detailed account of this theory and the experimental evidence that supports it as being a universal model for dipolar relaxation has been made by Jonscher.[39] This model is on sounder footing than the other dispersive models above in that it is capable of predicting

the temperature and time dependence of the amplitude of the response. Although this model was introduced to describe dielectric loss, we have used it to describe chromophore orientational relaxation in both the time and frequency domain, as will be discussed later in this paper. Unlike other decay models which assume the relaxing dipoles are non-interacting, the D-H model assumes just the opposite, that dipole relaxation is a highly cooperative process.[39] Additionally, the model statistically combines behavior in three frequency regimes. In high and low frequency regime, the dispersive behavior is described by a simple power law. Such a law has a firm basis in that, unlike the other empirical models, is consistent with Kramers-Kronig analysis, and thus, causality. In the transitional regime, the Dissado-Hill model yields the temperature and frequency dependence of the response amplitude which are absent in other models. The assumptions made in this model are that there are two preferred orientational states the dipoles, thus giving rise to a two level model. The potential energy diagram is shown in Figure 1.

In Figure 1, Δ is the height of the energy barrier that separates the two preferred states, and ξ denotes the width of correlated states. When an external electric field is applied to the dipolar dielectric media, the two potential well bottoms are split by an amount that depends not only on the strength of the applied electric field, but also on the occupancies of the two preferred energy states. There are three types of transitions that can occur, large thermal transitions, small flip transitions, and finally flip-flop or fluctuation transitions. The large transitions are thermally activated Debye-like transitions and thermally assisted tunneling processes that take a particle in one of the preferred states across or over the potential barrier into the other preferred state. Small flip transitions are tunneling transitions between the two preferred configurations that result in a net change of the total dipole moment, similar to the type of transitions Ngai *et al.*[40] had proposed. The final type of transitions, the flip-flop transitions can be described as local dipole moment fluctuations which involve the simultaneous tunneling of two particles between the two preferred states, but in opposite directions, resulting in no net change in the total dipole moment.

These three types of transitions are in competition with each other, and each has a time scale in which it is the dominant process. At times much shorter than $1/\omega_p$, where ω_p is a characteristic frequency in the Dissado-Hill model, the flip transitions are the dominant processes. At times approximately $1/\omega_p$, the dominant processes are the large thermal Debye-like transitions. Finally, at times much longer than $1/\omega_p$, the flip-flop or fluctuation transitions take over. The degree to which the flip transitions are correlated in a

particular dipolar media determines the shape of the frequency dependent dielectric loss curve at frequencies higher than ω_p. Similarly, the degree of correlation of the flip-flop transitions determines the shape of the loss curve at frequencies below ω_p.

The complete description of the dielectric loss curve as a function of frequency is a combination of these three processes, and can be written in terms of the Gaussian hypergeometric function, ${}_2F_1$,[41]

$$\chi(\omega) = \chi(0)\left(1 + i\omega/\omega_p\right)^{n-1} {}_2F_1\left(1-n \;;\; 2-m \;;\; 2-n; \left(1 + i\omega/\omega_p\right)^{-1}\right)$$

$$\begin{aligned} \chi''(\omega) &\propto \omega^{n-1}, && \omega >> \omega_p \\ \chi''(\omega) &\propto \mathrm{Im}\left(1 + i\omega/\omega_p\right)^{-1}, && \omega \cong \omega_p \\ \chi''(\omega) &\propto \omega^{m}, && \omega << \omega_p \end{aligned} \qquad (11)$$

Here n is a parameter that describes the degree of correlation of flip transitions, and m is a parameter that describes the degree of correlation of flip-flop transitions. Both parameters can range from zero to unity. As noted by Jonscher[39] the entire dielectric loss curve in the frequency domain can be broken up into three limiting regions. Near the loss peak, Debye loss mechanisms are still taking place in the dipolar media, and so the classical Debye function is still applicable. However, unlike the symmetric loss peak of the Debye model, asymmetric power law tails now appear in the loss spectrum both at higher and lower frequencies. The slopes of these power law tails depend on the parameters m and n. In this model, the relaxation time constant, τ, is defined as the inverse of the frequency of maximum loss and is determined from the parameters, m, n, and ω_p. The quantity ω_p only equals $1/\tau$ when n~1. The quantity τ will be used in temperature scaling of the structural relaxation in the data analysis below. By Fourier transforming Equation (11), one can obtain an expression for the depolarization current in the time domain in terms of the confluent hypergeometric function,[42]

$$i(t) = -\frac{dP(t)}{dt} \propto P'(0)\ \exp\left(-\omega_p t\right) t^{-m} {}_1F_1\left(1-m;\, 2-n;\, \omega_p t\right) \frac{\Gamma(1+m-n)}{\Gamma(2-n)\Gamma(1+m)}$$

$$\begin{aligned} i(t) &\propto t^{-m}, && t << 1/\omega_p \\ i(t) &\propto \exp\left(-\omega_p t\right), && t \cong 1/\omega_p \\ i(t) &\propto t^{-m-1}, && t >> 1/\omega_p \end{aligned} \qquad (12)$$

where $\dot{P}$ is the time rate of change of P, the macroscopic polarization of the media. Again, there is a Debye region at times near $1/\omega_p$, and two power law tails at times shorter and longer than $1/\omega_p$. The temperature dependence is implicit in the temperature dependence of ω_p.

In Figure 2, the KWW and D-H models are compared by choosing an appropriate log-log plot. It is apparent that both can fit the same data depending on the time scale examined. In addition, if the power law regions have nearly equal exponents (symmetric case), then the two models may be difficult to distinguish. We find with our frequency domain data below, that an asymmetric function is needed to fit the data. Thus, the D-H model is more general than the KWW model and is able to fit all of the data.

The advantage of the Dissado-Hill model over the previously discussed models is that it possesses a stronger physical basis being consistent with causality and by appropriately accounting for temperature and frequency dependence of the amplitude of the response. It is universal in that it has been applied to a wide variety of dipolar materials.[39] Also, it provides a theoretical description for dipolar relaxation in both the time and frequency domains. We have adapted it here to describe both dielectric and chielectric isothermal response spectra.

2.2. Structural Relaxation

Models for structural relaxation account for the temperature dependence of the characteristic time τ found in the reorientation models above. Though other parameters, namely n and m, are necessary to describe the time dependence of the reorientation, they are not as strongly temperature dependent as τ, and no good models exist for their temperature dependence. As above, the models used are drawn from the glass relaxation literature used to describe, for example, dielectric and mechanical relaxation. There have been several theoretical models introduced to describe the temperature dependence of the relaxation time constant based on entropy, free volume, or other phenomenological considerations.[43] Of these models, the three most widely used (along with closely related variations) are, the Williams-Landel-Ferry (WLF) model, an Arrhenius model, and the Adams-Gibbs model. The last model is the most general in that it yields the other two in appropriate temperature regions.

Stähelin *et al.*[44] investigating polyetherimides and BPDA-PDA polyimides doped with lophine chromophores, have found that τ is correlated to the glass transition temperature, T_g of the host polymer in the following manner.

$$\tau = \tau_0 \exp\left(\frac{B}{T_0 - T}\right) \tag{13}$$

where B and τ_0 are fitting parameters, and $T_0 \approx T_g + 50°C$. It should be noted that this type of temperature dependence is similar to Williams-Landel-Ferry (WLF) or Vogel-Fulcher (VF) expressions used to describe viscoelastic properties of polymers above T_g , and is appropriate only in that temperature range.[45,46]

Well below T_g, the nonlinear optical relaxation was found to follow Arrhenius behavior, consistent with other relaxation processes, in other words,[26]

$$\tau = \tau_0 \exp\left(-\frac{A}{kT}\right) \tag{14}$$

where A is the activation energy of the processes, and τ_0 is a parameter describing the activation entropy.

In the Adam-Gibbs entropic model of the glass transition, the structural relaxation of a polymer is the result of an increase in the number of molecular segments cooperatively rearranging as the temperature decreases.[47,48,49]

Tool originally modeled structural relaxation of polymers in terms of T_f, the fictive temperature.[50] The method for calculating T_f for a given polymeric glass was introduced by Narayanaswamy[51] and further developed by researchers such as Hodge[52] and Moynihan.[53,54] In terms of T_f, Hodge described the Adam-Gibbs type temperature dependence of the relaxation time constant as

$$\tau = A \exp\left(\frac{B}{T\left(1 - T_2/T_f\right)}\right) \tag{15}$$

or scaling τ to it's value at the glass transition temperature.

$$\tau = \tau_g \exp\left(B\left(\frac{1}{T\left(1 - T_2/T_f\right)} - \frac{1}{T_g - T_2}\right)\right) \tag{16}$$

where τ_g is the relaxation time constant at the glass transition temperature. B is an activation energy, A is a time scaling parameter, and T_2 is the zero point configurational entropy temperature. The physical meaning of the fictive temperature is shown in Figure 3. At temperatures above the glass transition temperature, $T_f \sim T$, and the expression for τ reduces to,

$$\tau/\tau_g = \exp\left(B\left(\frac{1}{T - T_2}\right) - \frac{1}{T_g - T_2}\right) \tag{17}$$

which is just the Fulcher-Tammann-Hesse or the equivalent Williams-Landel-Ferry expression.[55] Below T_g, T_f approaches T_g and

$$\tau/\tau_g = \exp\left(\frac{B}{T_g - T_2}\frac{T_g - T}{T}\right) \tag{18}$$

which is an equivalent expression for Arrhenius temperature behavior. Thus, the Adam-Gibbs model provides a more general description of the temperature dependence of τ, because it can be used to describe relaxation both above and below the glass transition temperature.

3. Experimental technique

3.1. Material Preparation

The polymer systems studied in this work included two guest-host systems, namely DR1/PMMA and DCM/PMMA, and one side chain system, DR1-MMA.[56] The glass transition temperatures of these materials were measured using differential scanning calorimetry (DSC) and are listed in Figure 4 along with their molecular structures. Samples were prepared by spin coating solutions of the chromophore and polymer onto ITO coated sapphire substrates and baking at T_g+ 30 °C for several hours yielding 2μm thick films that consisted of 10% by weight of chromophore. Next, two coated substrates were placed in a sandwich configuration and fused under pressure for two hours at a temperature above the polymer's glass transition temperature. The pressure rig was designed to apply the same pressure to all samples. Then the pressure was removed and the sandwiched film was annealed for one hour at an elevated temperature of

T_g+30C to relieve any built up stresses in the sample. Consistent thermal histories were applied in all cases.

3.2. Chromophore reorientation measurements

Measuring chromophore orientational relaxation is accomplished by monitoring the macroscopic polarization of a NLO polymer system, or to be more precise, by monitoring the linear, $\chi^{(1)}$, and nonlinear, $\chi^{(2)}$, susceptibilities. There are basically four types of experiments that can be performed on polymeric media that measure these tensors, two of which probe $\chi^{(1)}$, and two that probe $\chi^{(2)}$. The two experiments that probe $\chi^{(1)}$ are dielectric loss measurements in the frequency domain, and depolarization current measurements in the time domain, which monitor the time rate of change of the polarization. As for the $\chi^{(2)}$ experiments, these are SH decay measurements in the time domain and chielectric relaxation measurements in the frequency domain.[57] Time domain measurements are more appropriate at long time scales, and frequency at shorter time scales, and the combination allows a wide range of time scales to be probed. To minimize sample to sample measurement variation, all four experiments were performed on the same sample. To analyze the experimental results, the Dissado-Hill model was chosen, because it provided the best fit to both the time domain and frequency domain data in all cases.

The experimental setup used for time domain measurements is shown in Figure 5. In this configuration, both the SH light generated from the chromophores and the depolarization current can be measured simultaneously. SH measurements were made by focusing intense laser light from a Ti:Sapphire source onto a contact poled sample. The 100 MHz mode-locked Ti:Sapphire Argon ion pumped laser produced 50 fs pulses as measured by an autocorrelator with an average output power of approximately 700mw and a 780nm peak wavelength. After the fundamental light was filtered out, the SH light generated from the sample was collected and focused onto a Hammamatsu avalanche photodiode. The electrical signal from the photodiode was monitored using a Stanford Research SRS850 dual phase lock in amplifier whose reference frequency was generated from an optical chopper. The depolarization current was monitored using a Hewlett-Packard 6517 electrometer that also served as the voltage source for poling the sample.

Dielectric measurements were made using a CGA-83 ratio-arm transformer bridge. The frequency range investigated was from 10 Hz to 100 kHz and the temperature range was again near Tg for all samples.

Chielectric relaxation, or frequency domain electric field induced second harmonic generation, is a relatively new technique introduced by J.A. Cline and W.N. Herman to observe chromophore relaxation in the frequency domain.[57] Their method is similar to dielectric relaxation measurements that use a sinusoidal electric field to probe the linear dielectric response, but differs in that it measures the second harmonic (SH) light generated from the relaxing chromophores to probe the nonlinear optical susceptibility. The advantage of the chielectric relaxation measurements is that the measured SH response is entirely due to the chromophore, while in the dielectric case, both the chromophore and polymer contribute to the dielectric response. It is also easily connected to the time domain measurements of SHG so that time scales over many decades can be probed.

Using a mode-locked Ti:Sapphire laser, a more quantitative analysis of frequency domain chromophore relaxation has been made. Broadening the frequency range to include frequencies from 10 mHz to 40 kHz, has allowed measurements to be made at temperatures from slightly below T_g to temperatures far above T_g.

The chielectric frequency domain experimental setup is nearly the same as the time domain setup, except for a few variations as shown in Figure 6. SH measurements were made by applying a sinusoidal voltage (~400 V_{pp}) to the sample's ITO electrodes while the intense laser light from a Ti:Sapphire source was focused onto the sample. After the fundamental light was filtered out, the SH light generated from the sample was again collected and focused onto a Hammamatsu avalanche photodiode. The electrical signal from the photodiode was monitored using a Stanford Research SRS850 dual phase lock in amplifier which also served as the sine wave generator for the applied voltage. The frequency range examined in this work was from 10 mHz to 40 kHz, and the temperature range was near Tg for all samples.

The assumption is made that the second order nonlinear optical susceptibility varies linearly with respect to the applied electric field, which means if the applied field has a sinusoidal time dependence, $\chi^{(2)}$ can be rewritten as,

$$\chi^{(2)} = A\sin(\omega t + \phi) \tag{19}$$

where ω is the frequency of the applied field and ϕ is the phase lag of the chromophore orientation with respect to the applied field. Since the SH intensity varies as the square of $\chi^{(2)}$,

$$I^{2\omega} \propto \left(A\sin\left(\omega t+\phi\right)\right)^2 = \frac{A^2}{2}\left(1-2\cos\left(2\left(\omega t+\phi\right)\right)\right). \tag{20}$$

Thus, by setting a lock-in amplifier to lock in at twice the applied voltage frequency, both the in phase component and the out of phase component of $\chi^{(2)}$ can be measured directly.

The fictive temperature was determined using a TA Instruments DSC 2910 differential scanning calorimeter. Rate cooling heat capacity measurements were performed on all three of the polymer systems in this study following the procedure outlined by DeBolt et al.[54] In rate cooling heat capacity experiments, the polymer sample is first heated above the glass transition temperature, then cooled below T_g at a constant rate, and finally heated at 20 °C/min through T_g. This thermal cycle was repeated for several different cooling rates ranging from 20 °C/min to .5 °C/min. From the heat capacity data obtained from these sets of experiments, the temperature dependence of the fictive temperature, T_f, was determined using the relationship between the heat capacity and the temperature rate of change of T_f,

$$\frac{dT_f}{dT} = \frac{C_p(T)-C_{pg}(T)}{C_{pe}(T)-C_{pg}(T)}$$

where C_{pg} and C_{pe} are the extrapolated heat capacities in the glassy and equilibrium temperature regions.

Results and Discussion

Upon removal of the poling field, the magnitude of $\chi^{(2)}$ will begin to decay. This decay can be monitored by measuring the intensity of SH light generated from the relaxing chromophores. For the dye molecules in our studies there are only two nonzero tensor elements of $\chi^{(2)}$: $\chi^{(2)}{}_{311}$ and $\chi^{(2)}{}_{333}$. For our measurements we arranged the geometric setup such that we are coupling to the $\chi^{(2)}{}_{333}$ element, and so we have the following expression for the intensity of SH light,

$$\begin{aligned} I^{2\omega} &\propto \left|\chi^{(2)}_{333}\right|^2 \\ \chi^{(2)}_{333} &\propto \beta_{333}\left\langle\cos^3\theta\right\rangle = \beta_{333}\left(\frac{2}{5}\left\langle P_3(\cos\theta)\right\rangle + \frac{3}{5}\left\langle P_1(\cos\theta)\right\rangle\right) \approx \beta_{333}\left\langle\cos\theta\right\rangle \end{aligned} \tag{22}$$

where $I^{2\omega}$ is the SH light intensity, β_{333} is the molecular second order hyperpolarizability tensor element, and θ is the angle the relaxing dye molecule makes with the direction of the poling field.[58,59] The final expression for $\chi^{(2)}_{333}$ was made by expanding in terms of Legendre polynomials and then approximating in terms of $\langle\cos\theta\rangle$.[60] Note that Equation (22) indicates that the dielectric and nonlinear optic experiments mainly probe the same order parameter, however, the nonlinear optic measurement probes only the nonlinear optical chromophore. An example decay curve for DR1\PMMA is shown in Figure 7. It is clear from the data, that neither a single nor double exponential would fit the data. At the same time the SH decay was being measured, the depolarization current caused by the rotating dipoles of the relaxing chromophores was also being monitored. In theory the current being measured should be entirely due to the time rate of change of the macroscopic polarization, however, low frequency dispersion (LFD) was found in all of the samples studied. The primary source of LFD is probably due to trapped charges being released. An example of the depolarization current data is shown in Figure 8. The kink at long times corresponds to the LFD due to trapped charges.

As previously mentioned, dielectric measurements were carried out in the frequency range from 10 Hz to 100 kHz. A detailed account of the basic theory behind dielectric relaxation can be found in texts by Jonscher[39] or McCrum.[61] The in phase and out of phase components of the dielectric spectra for the three NLO polymer systems studied are shown in Figure 9. Both α and β peaks are visible in the loss spectra. The peak of the imaginary part of the dielectric constant determines the characteristic frequency which is a fit parameter in the D-H model. It is clear that the characteristic frequency depends strongly on temperature. This dependence will be compared to the Adams-Gibbs relaxation model below.

Figure 10 shows the measured $\chi^{(2)}$ components for the three NLO polymer systems in this study. We see close agreement between the dielectric measurements and chielectric spectra, and with the D-H model fits. We also determined that the spectra are linear in the electric field as expected from Equation (19) and shown in Figure 11. This linearity indicates that trapped volume or surface charges are not contributing in these measurements. In time domain SHG measurements, the trapped charges may affect the decay. However, we have carefully shorted the electrodes as the poling field was turned off and did not see any obvious effect of trapped charges. Further evidence for this is given below where the time domain and frequency domain measurements are found to closely correspond.

The data collected from all four sets of experiments were analyzed within the framework of the Dissado-Hill many body universal relaxation model. As previousiy stated, this model was chosen not only because it provided a better fit to experimental data, but also because it is not entirely empirical, and has analytical relaxation expressions for both the time and frequency domains. In calculating the relaxation time constant, τ, for the time domain measurements, the experimental data was fit to the time domain Dissado-Hill depolarization current expression from Equation (12). From this, the three Dissado-Hill parameters n, m, and ω_p were determined and inserted into Equation (11) to calculate the frequency of maximum loss, i.e. the reciprocal of τ. For the frequency domain experiments, the data was fit directly to Equation (11) to calculate τ. Putting all four sets of experimental data together, a plot of the temperature dependence of τ is shown in Figure 12 for the DR1\PMMA of polymer system. It should be noted that while the dielectric measurements show both an α and β relaxation, the chielectric data shows only one relaxation that overlaps the dielectric α relaxation data. This suggests that chromophore relaxation is strongly coupled to the α relaxation of the polymer host. To monitor the structural relaxation of the polymer host the temperature dependence of the fictive temperature is calculated from the rate cooling enthalpy experiments. Example enthalpy results are shown in Figure 13.

In Figure 14, the temperature dependence of τ for all three polymer systems are superimposed on one plot. For each system, the temperature is scaled to the respective glass transition temperature. By scaling the temperature with respect to T_g of each system, the measured τ values from the α relaxations appear to lie on a single master curve as suggested by other studies.[33] This leads to predictive capabilities for the useful lifetime of the electro-optic properties of polymer-chromophore systems. It is also apparent in Figure 14 that all four techniques yield consistent results, and are thus likely probing the same physical mechanisms. This suggests that real charge effects are not seen under these experimental conditions.

Also in Figure 14, the Adam-Gibbs theoretical fit with T_f calculated from the DR1-MMA enthalpy data , along with Arrhenius and WLF fits have been superimposed on the experimental data. The WLF curve fits the data above Tg and the Arrhenius curve fits the data below Tg, the Adam-Gibbs curve fits the data in all temperature ranges.

4. Conclusion

By combining results from both time and frequency domain experiments, a complete description of chromophore relaxation in polymeric media can be determined. Using the Dissado-Hill many body universal relaxation model to extract the relaxation time constant, τ, from the data, and the Adam-Gibbs formalism to describe the temperature dependence of τ, we have found good agreement between experiment and theory over 13 orders of magnitude in time and over temperatures that ranged from far below T_g to far above it. We have also shown that chromophore relaxation is coupled primarily to the α relaxation of the host polymer. In addition, after scaling the temperature to T_g and the relaxation time constant, τ, to τ_g, the calculated values for τ for all three types of polymeric systems in this study, seem to have the same reduced temperature dependence which indicates this type of relaxation behavior may be universal, at least within the same types of glass forming polymers. We have also further developed the chielectric relaxation experimental technique for measuring chromophore reorientation in the frequency domain, and have shown how it can be used to directly study the relaxation mechanism in the chromophores.

Currently we are investigating a wider variety of NLO polymeric media, including higher T_g guest/host systems, polyimides, and also cross-linked polymers, to determine if the results found in this limited study can be applied in general. If they can, the techniques discussed here may prove to be a useful tool in predicting which NLO media will be viable in device applications.

5. Acknowledgements

This work was supported by the Air Force Office of Scientific Research grant No. F49620-93-1-0202, and by the National Science Foundation under the Science and Technology Center for Advanced Liquid Crystalline Optical Materials grant No. DMR89-20147.

References

[1] G.A. Lindsay and K.D. Singer, "Polymers for Second-Order Nonlinear Optics", ACS Symp. Ser. 601, American Chemical Society, Washington, D.C. (1995).

[2] D.M. Burland, R.D. Miller, and C.A. Walsh, "Second-Order Nonlinearity in Poled-Polymer Systems", Chem. Rev. **94**, 31-75 (1994).

[3] R. Lytel, G. F. Lipscomb, J. T. Kenney, and E. S. Binkley, "In Polymers for Lightwave and Integrated Optics", ed. L. A. Hornack, Marcel Dekker, New York (1992).

[4] G. Meredith, J. VanDusen, and D. Williams, "Optical and Nonlinear Optical Characterization of Molecularly Doped Thermotropic Liquid Crystalline Polymers", Macromolecules **15**, 1385-1389 (1982).

[5] K.D. Singer, J.E. Sohn, and S. J. Lalama, "Second harmonic generation in poled polymer films", Appl. Phys. Lett. **49**, 248-250 (1986).

[6] C. Ye, T.J. Marks, J. Yang, and G.K. Wong, "Synthesis of Molecular Arrays with Nonlinear Optical-Properties - 2nd-Harmonic Generation by Covalently Functionalized Glassy-Polymers", Macromolecules **20**, 2322-2324 (1987).

[7] H.L. Hampsch, J. Yang, G.K. Wong, and J.M. Torkelson, "Orientation and 2nd Harmonic-Generation in Doped Polystyrene and Poly(Methyl Methacrylate) Films", Macromolecules **21**, 526-528 (1988).

[8] P. Debye, "Polar Molecules", Lancaster Press Inc., PA (1929).

[9] D. J. Williams,"Nonlinear Optical Properties of Guest-Host Polymer Structures", Nonlinear Optical Properties of Organic Molecules and Crystals **1**, ed. D. S. Chemla and J. Zyss, Academic Press, Inc., New York (1987).

[10] H. L. Hampsch, J. M. Torkelson, S. J. Bethke, and S. G. Grubb, "2nd Harmonic-Generation in Corona Poled, Doped Polymer-Films As a Function of Corona Processing", J. App. Phys. **67**, 1037-1041 (1990).

[11] C. H. Wang, S. H. Gu, and H. W. Guan, "Polar Order and Relaxation of 2nd-Order Nonlinear-Optical Susceptibility in an Electric-Field Polarized Amorphous Polymer", J. Chem. Phys. **99**, 5597-5604 (1993).

[12] M. Eich, H. Looser, D.Y. Yoon, R. Twieg, G. C. Bjorklund, and J.C. Baumert, "2nd-Harmonic Generation in Poled Organic Monomeric Glasses", J. Opt. Soc. Am. B **6**, 1590-1597 (1989).

[13] C. G. Garton, "The Distribution of Relaxation Times in Dielectrics", Trans. Far. Soc. XLII A. 56-60 (1946).

[14] H. Fröhlich, "Theory of Dielectrics: Dielectric Constant and Dielectric Loss", Clarendon Press, Oxford (1949).

[15] J. R. Macdonald, "Some Statistical Aspects of Relaxation Time Distributions", Physica **28**, 485-492 (1962).

[16] J. R. Macdonald, "Restrictions on the Form of Relaxation Time Distribution Functions for a Thermally Activated Process", J. Chem. Phys. **36**, 345-349 (1962).

[17] J. R. Macdonald, "Transient and Temperature Response of a Distributed, Thermally Activated System", J. Appl. Phys. **34**, 538-552 (1963).

[18] C. J. Böttcher and P. Bordewijk, "Theory of Electronic Polarisation", Vol. 2, Elsevier, Amsterdam (1978).

[19] H. L. Hampsch, J. M. Torkelson, J. Yang, and G. K. Wong, "2nd Harmonic-Generation in Doped Glassy Polymer-Films As a Function of Physical Aging and Dopant Size", Poly. Commun. **30**, 40-43 (1989).

[20] C. P. J. M van der Vorst, and R. A. P. van Gassel, "Thermal Relaxation of Poled Non-Linear Optical Sidechain Polymers: A New, Semi-empirical Model", Macromolecular Symposia **90**, 47-64 (1994).

[21] T. Goodson, and C. H. Wang, "Dipolar Orientational Relaxation in Guest Host Amorphous Polymer Probed by 2nd-Harmonic Generation", Macromolecules **26**, 1837-1840 (1993).

[22] H. L. Hampsch, J. Yang, G. K. Wong, and J. M. Torkelson, "Dopant Orientation Dynamics in Doped 2nd-Order Nonlinear Optical Amorphous Polymers .1. Effects of Temperature Above and Below Tg in Corona-Poled Films", Macromolecules **23**, 3640-3647 (1990).

[23] R. Kohlrausch, Ann. Phys. Leipzig, **12**, 393 (1847).

[24] G. Williams, and D. C. Watts, "Non-symmetrical Dielectric Relaxation Behaviour Arising from a Simple Empirical Decay Function", Trans. Far. Soc. **66**, 80-85 (1970).

[25] M. G. Kuzyk, R. C. Moore, and L. A. King, "2nd-Harmonic-Generation Measurements of the Elastic-Constant of a Molecule in a Polymer Matrix", J. Opt. Soc. Am. B **7**, 64-72 (1990).

[26] K. D. Singer and L. A. King, "Relaxation Phenomena in Polymer Nonlinear Optical-Materials", J. Appl. Phys. 70, 3251-3255 (1991).

[27] A. Dhinojwala, G. K. Wong, and J. M. Torkleson, "Rotational Reorientation Dynamics of Nonlinear-Optical Chromophores in Rubbery and Glassy-Polymers - Alpha-Relaxation Dynamics Probed by 2nd-Harmonic Generation and Dielectric-Relaxation", Macromolecules **26**, 5943-5953 (1993).

[28] J. Klafter and M. F. Shlesinger, "On the Relationship Among Three Theories of Relaxation in Disordered Systems", Proc. Natl. Acad. Sci. **83**, 848-851 (1986).

[29] K. Weron, "A Probabilistic Mechanism Hidden Behind the Universal Power Law for Dielectric-Relaxation - General Relaxation Equation", J. Phys. : Condens. Matter **3**, 9151-9162 (1991).

[30] M. F. Shlesinger and J. Klafter, "Fractal in Physics", ed. L.P. Pietronero and E. Tosatti , North-Holland, Amsterdam 393 (1986).

[31] F. Ghebremichael, and M. G. Kuzyk, "Optical second-harmonic generation as a probe of the temperature dependence of the distribution of sites in a poly(methyl methacrylate) polymer doped with disperse red 1 azo dye", J. Appl. Phys. 77, 2896-2901 (1995).

[32] A. Dhinojwala, G. K. Wong, and J. M. Torkleson, "Rotational Reorientation Dynamics of Disperse Red-1 in Polystyrene - Alpha-Relaxation Dynamics Probed by 2nd-Harmonic Generation and Dielectric-Relaxation", J. Chem. Phys. **100**, 6046-6054 (1994).

[33] P. Kaatz, P. Pretre, U. Meier, C. Bosshard, P. Gunter, B. Zysset, M. Stahelin, M. Ahlheim, and F. Lehr, "Relaxation in Nonlinear Optical Polyimide Side-Chain Polymers", Macromolecules **29**, 1666-1678 (1996).

[34] J. Wu, "Birefringent and electro-optic effects in poled polymer films: steady-state and transient properties", J. Opt. Soc. Am. B **8**, 142-152 (1991).

[35] S. C. Brower, L. M. Hayden, "Activation Volume Associated with the Relaxation of the 2nd-Order Nonlinear-Optical Susceptibility in a Guest-Host Polymer", Appl. Phys. Lett. **63**, 2059-2061 (1993).

[36] L. Liu, D. Ramkrishna, and H. S. Lackritz, "Rotational Brownian-Motion of Chromophores and Electric-Field Effects in Polymer-Films for 2nd-Order Nonlinear Optics", Macromolecules **27**, 5987-5999 (1994).

[37] T. Verbiest, and D. M. Burland, "The use of the Wagner function to describe poled-order relaxation processes in electrooptic polymers", Chem. Phys. Lett., **236**, 253-258 (1995).

[38] L. A. Dissado, R. M. Hill, "Non-exponential decay in dielectrics and dynamics of correlated systems", Nature, **279**, 685-689 (1979).

[39] A. K. Jonscher, "Dielectric Relaxation in Solids", Chelsea Dielectrics Press Ltd., London (1983).

Material	T_g (°C)	Molecular Structure
PMMA	110	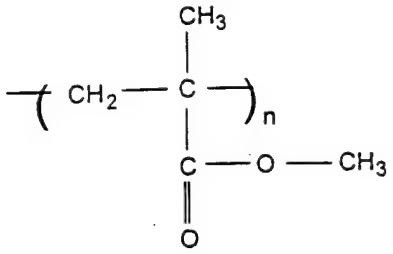
DCM\PMMA	97	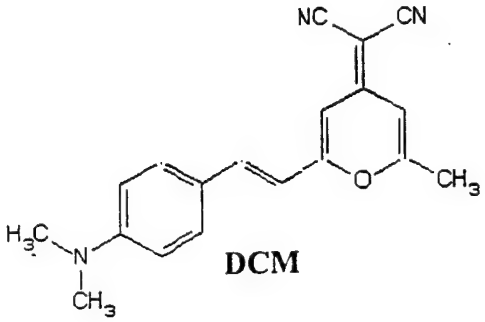 DCM
DR1\PMMA	90	 DR1
DR1-MMA	125	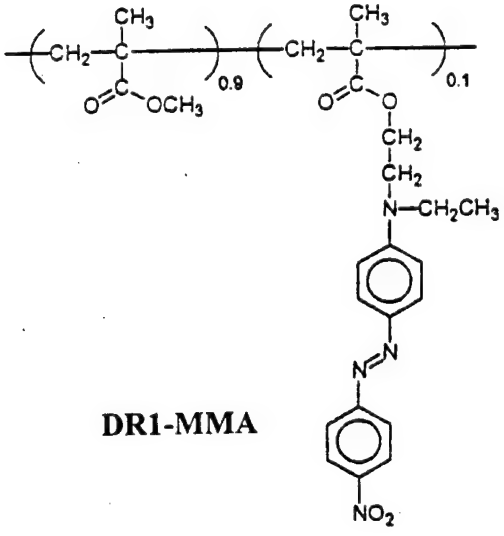 DR1-MMA

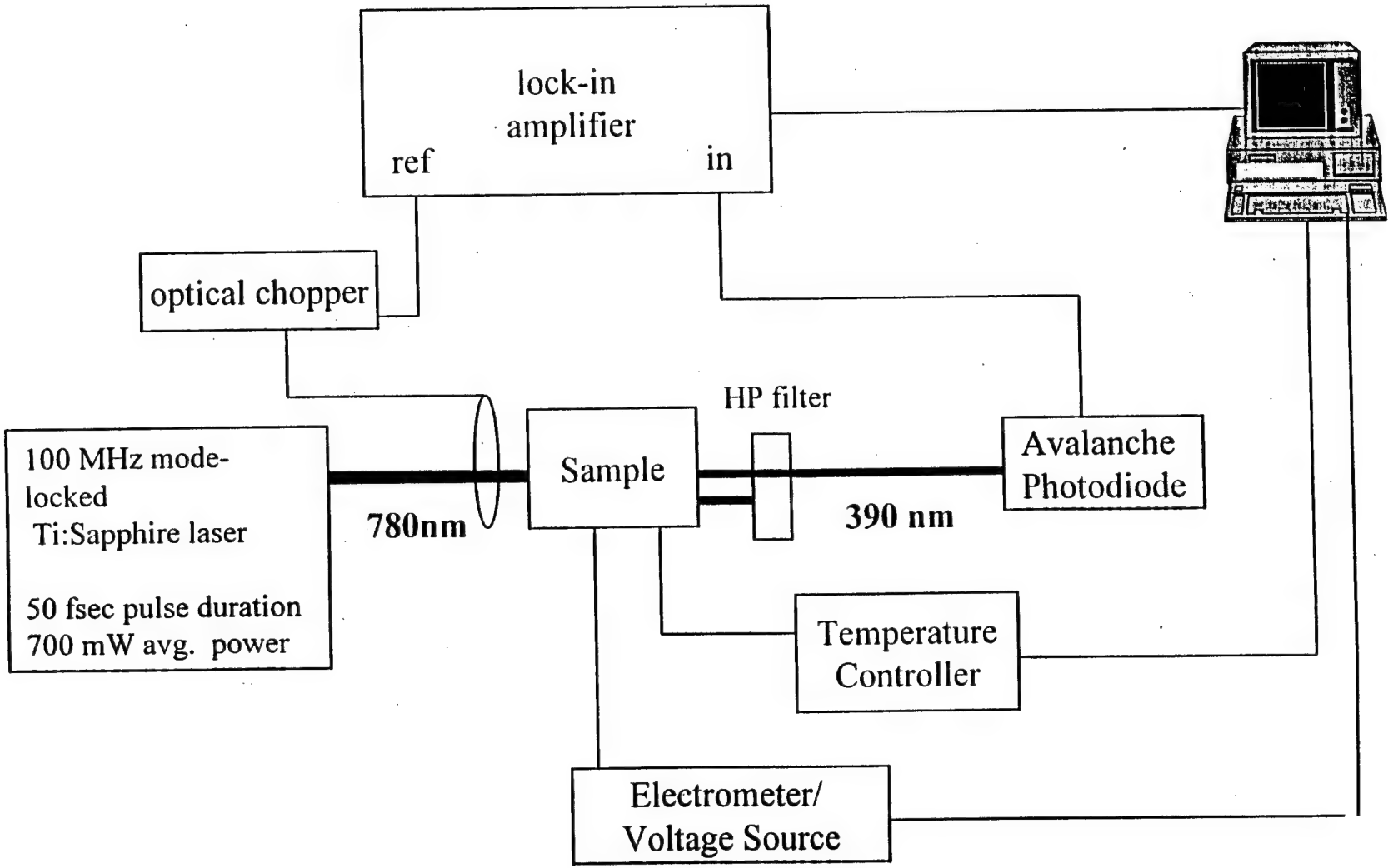
lock-in
amplifier
ref
in
optical chopper
HP filter
100 MHz mode-
locked
Ti:Sapphire laser
50 fsec pulse duration
700 mW avg. power
780nm
Sample
390 nm
Avalanche
Photodiode
Temperature
Controller
Electrometer/
Voltage Source

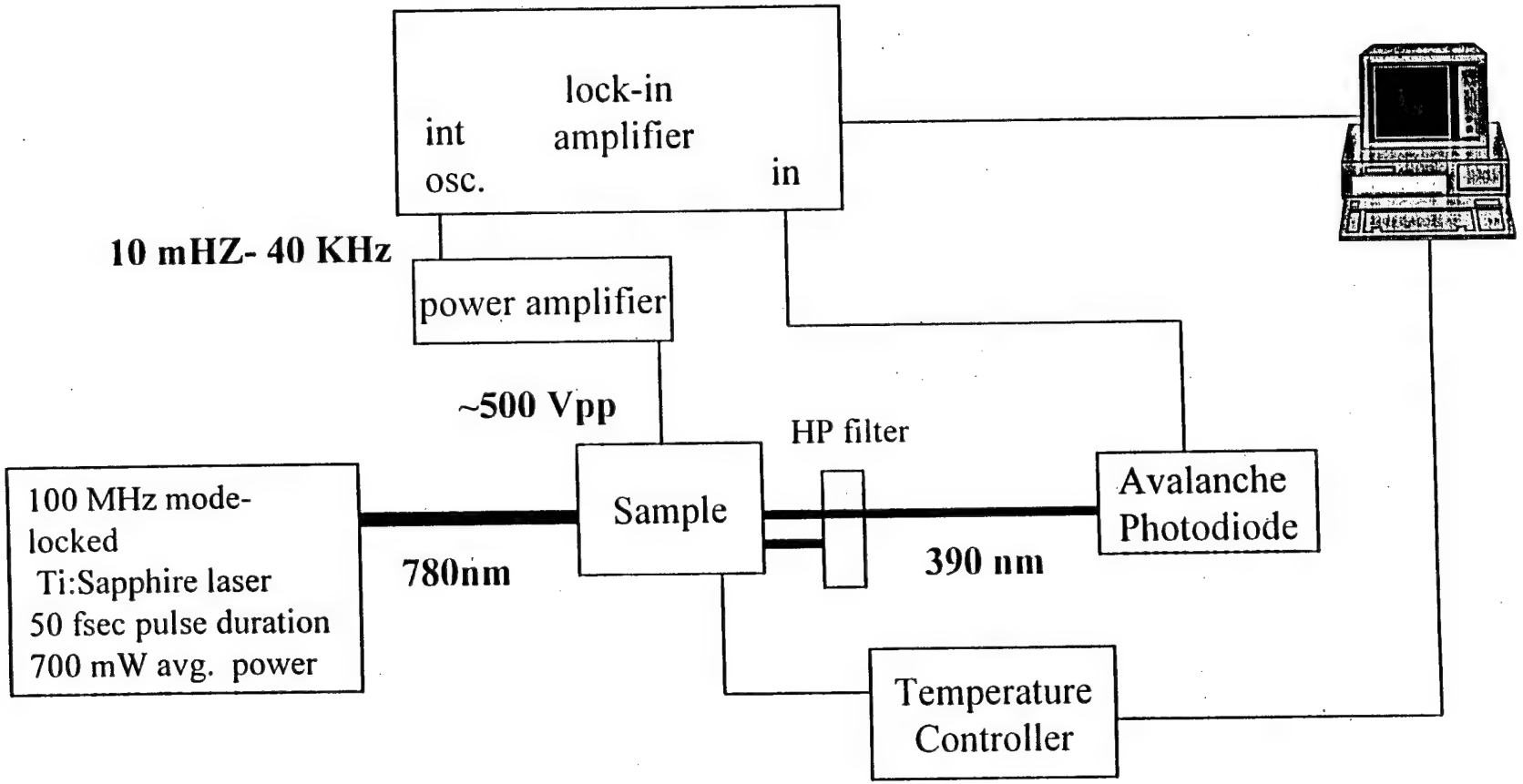
lock-in
amplifier
int
osc.
in
10 mHZ- 40 KHz
power amplifier
~500 Vpp
HP filter
100 MHz mode-
locked
Ti:Sapphire laser
50 fsec pulse duration
700 mW avg. power
780nm
Sample
390 nm
Avalanche
Photodiode
Temperature
Controller

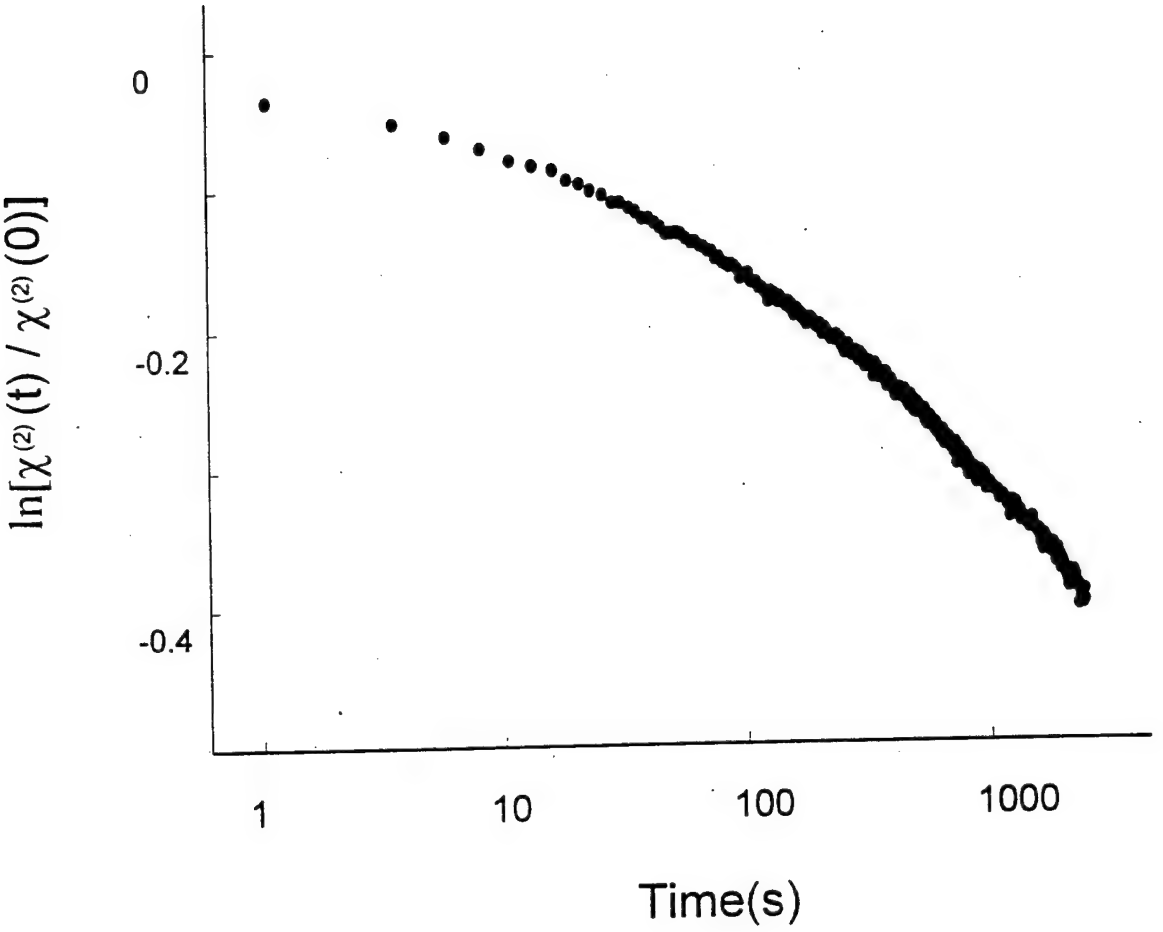
0
-0.2
-0.4
ln[χ(2) (t) / χ(2) (0)]
1
10
100
1000
Time(s)

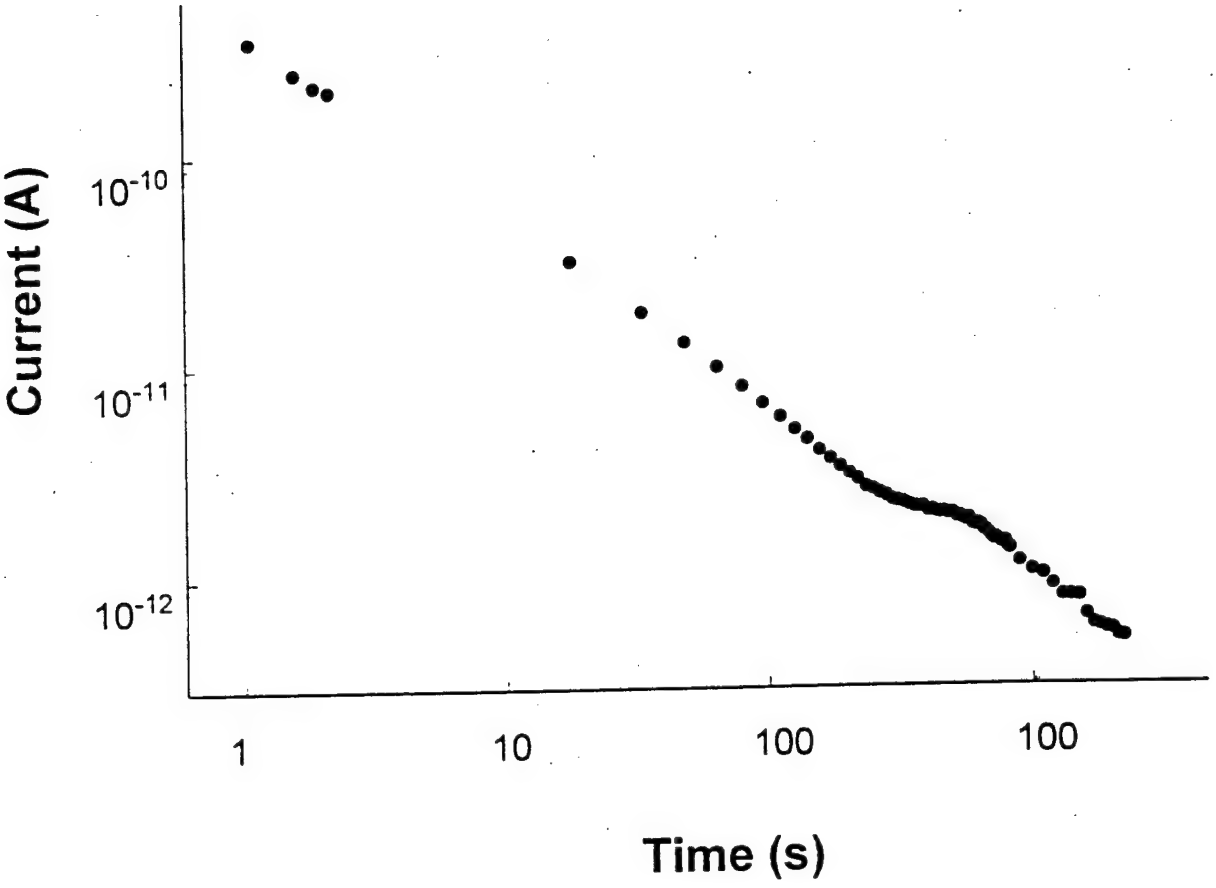
Current (A)
10-10
10-11
10-12
1
10
100
100
Time (s)

(a)

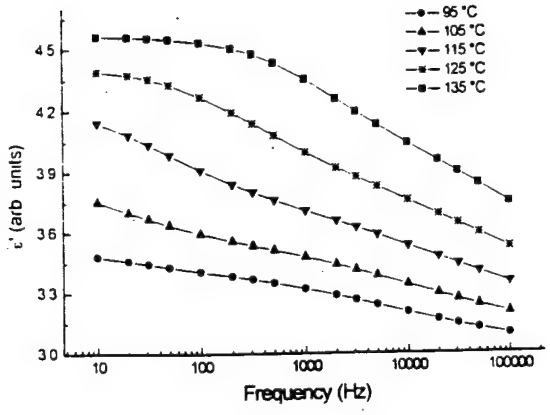
95 °C
105 °C
115 °C
125 °C
135 °C
ε' (arb. units)
Frequency (Hz)

(b)

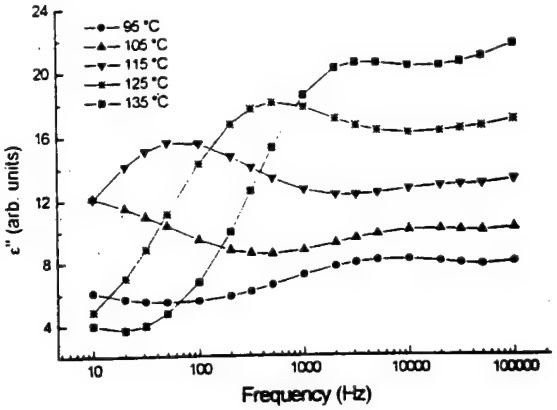
95 °C
105 °C
115 °C
125 °C
135 °C
ε'' (arb. units)
Frequency (Hz)

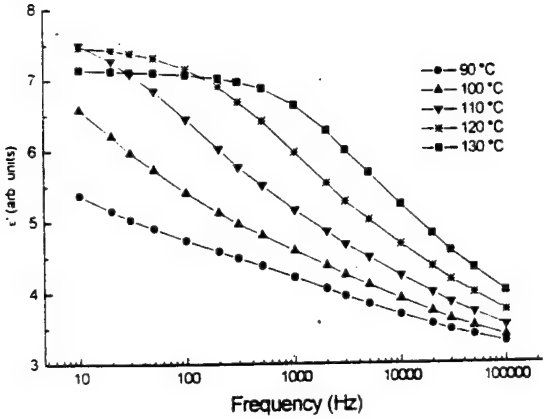
90 °C
100 °C
110 °C
120 °C
130 °C
ε' (arb. units)
Frequency (Hz)

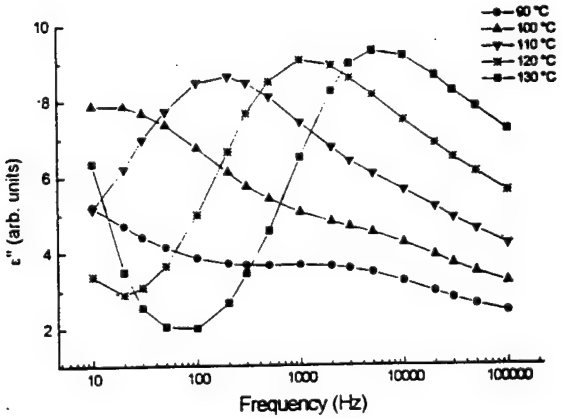
90 °C
100 °C
110 °C
120 °C
130 °C
ε'' (arb. units)
Frequency (Hz)

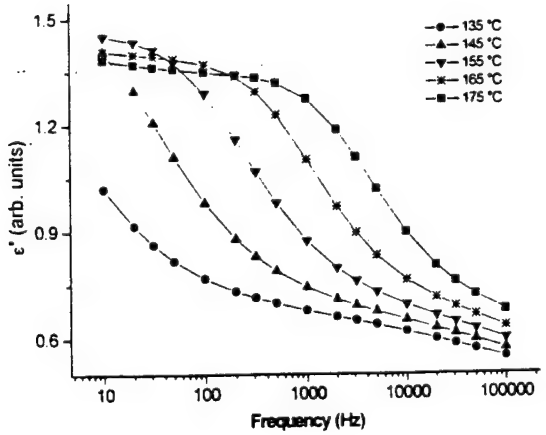
135 °C
145 °C
155 °C
165 °C
175 °C
ε' (arb. units)
Frequency (Hz)

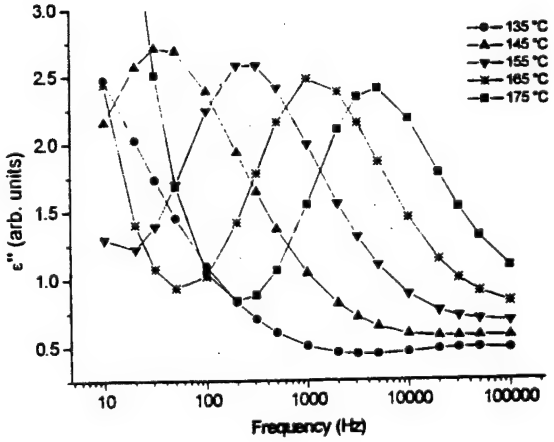
135 °C
145 °C
155 °C
165 °C
175 °C
ε'' (arb. units)
Frequency (Hz)

(a)

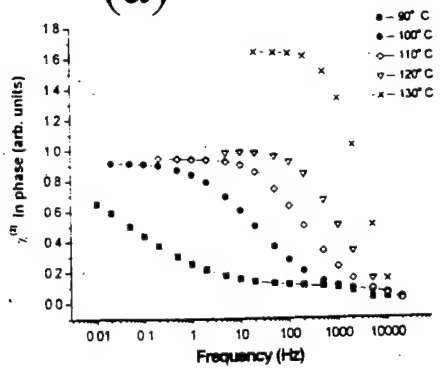
90° C
100° C
110° C
120° C
130° C
χ(3) in phase (arb. units)
Frequency (Hz)

(b)

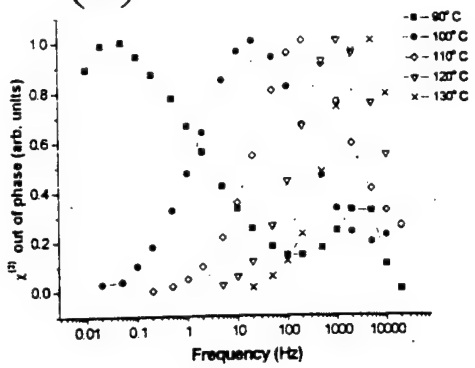
90° C
100° C
110° C
120° C
130° C
χ(3) out of phase (arb. units)
Frequency (Hz)

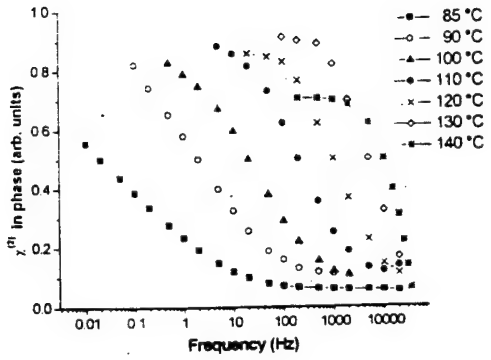
85 °C
90 °C
100 °C
110 °C
120 °C
130 °C
140 °C
χ(3) in phase (arb. units)
Frequency (Hz)

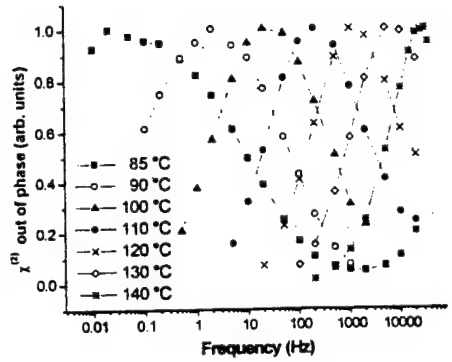
85 °C
90 °C
100 °C
110 °C
120 °C
130 °C
140 °C
χ(3) out of phase (arb. units)
Frequency (Hz)

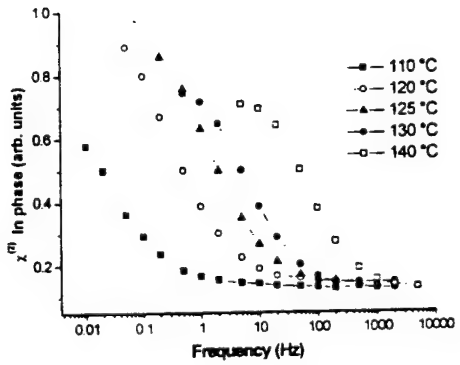
110 °C
120 °C
125 °C
130 °C
140 °C
χ(3) in phase (arb. units)
Frequency (Hz)

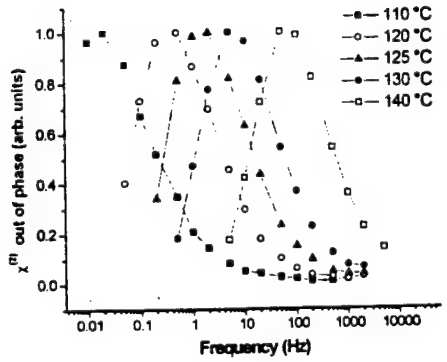
110 °C
120 °C
125 °C
130 °C
140 °C
χ(3) out of phase (arb. units)
Frequency (Hz)

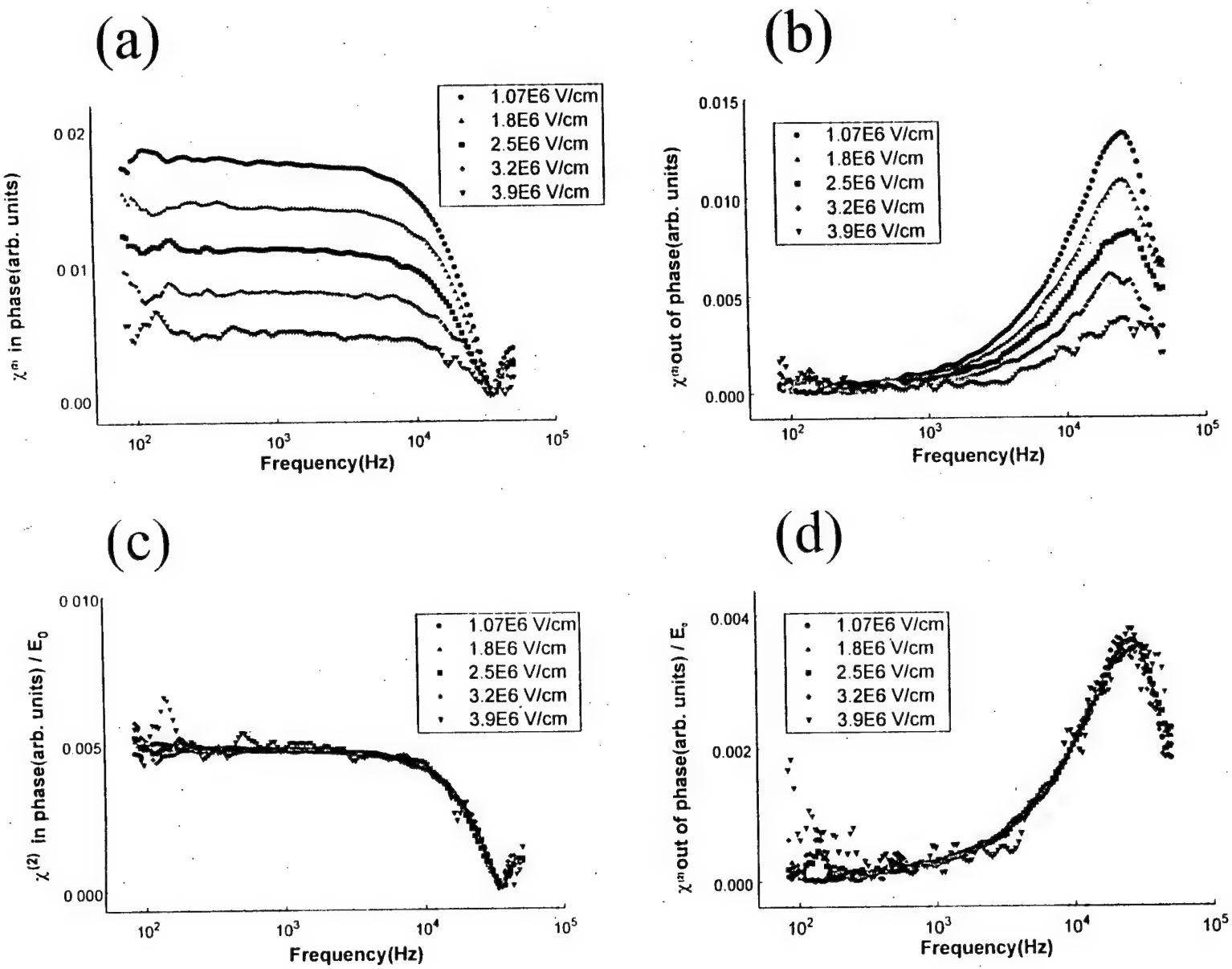
(a)
1.07E6 V/cm
1.8E6 V/cm
2.5E6 V/cm
3.2E6 V/cm
3.9E6 V/cm
0 02
0 01
0.00
χ(2) in phase(arb. units)
10^2
10^3
10^4
10^5
Frequency(Hz)
(b)
0.015
0.010
0.005
0.000
χ(2) out of phase(arb. units)
Frequency(Hz)
(c)
0 010
0.005
0 000
χ(2) in phase(arb. units) / E0
Frequency(Hz)
(d)
0.004
0.002
0.000
χ(2) out of phase(arb. units) / E0
Frequency(Hz)

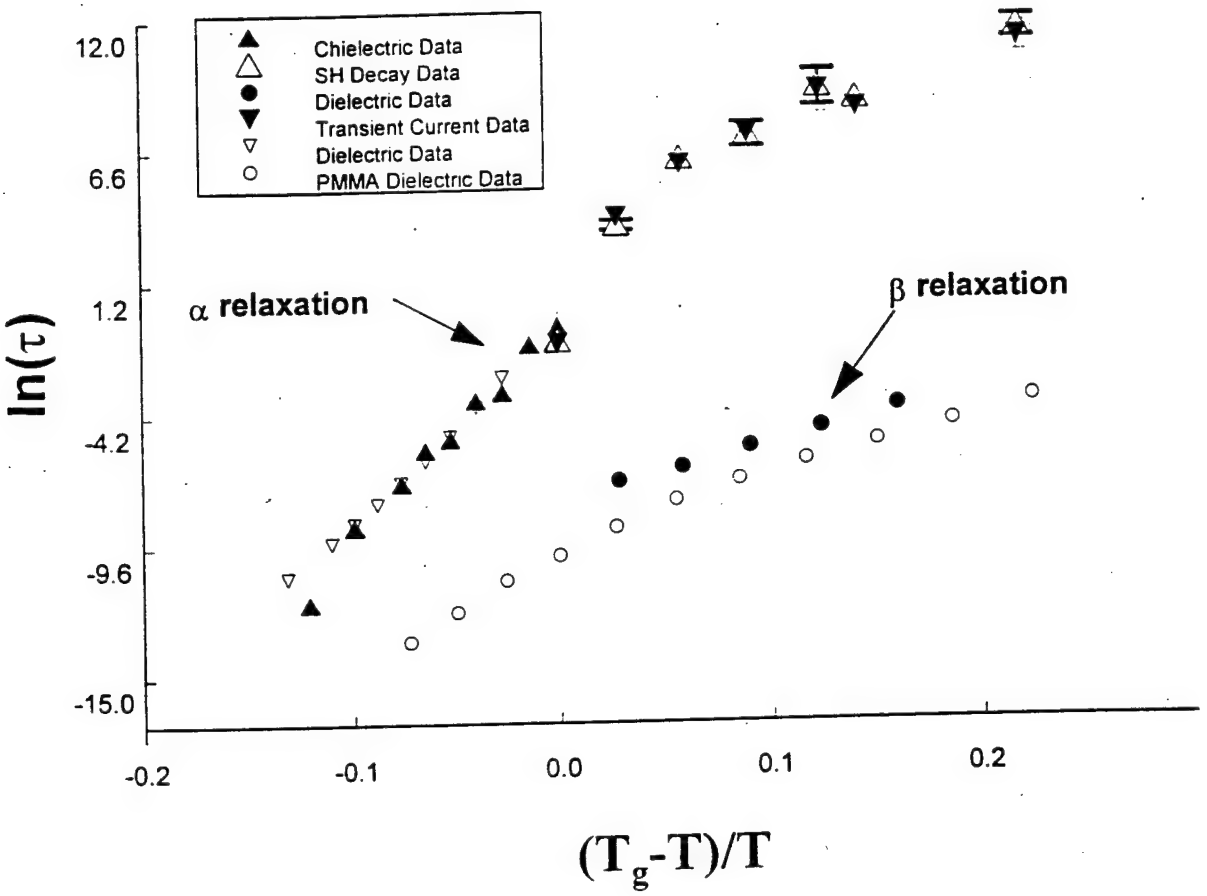
Chielectric Data
SH Decay Data
Dielectric Data
Transient Current Data
Dielectric Data
PMMA Dielectric Data
α relaxation
β relaxation
ln(τ)
12.0
6.6
1.2
-4.2
-9.6
-15.0
-0.2
-0.1
0.0
0.1
0.2
(T_g-T)/T

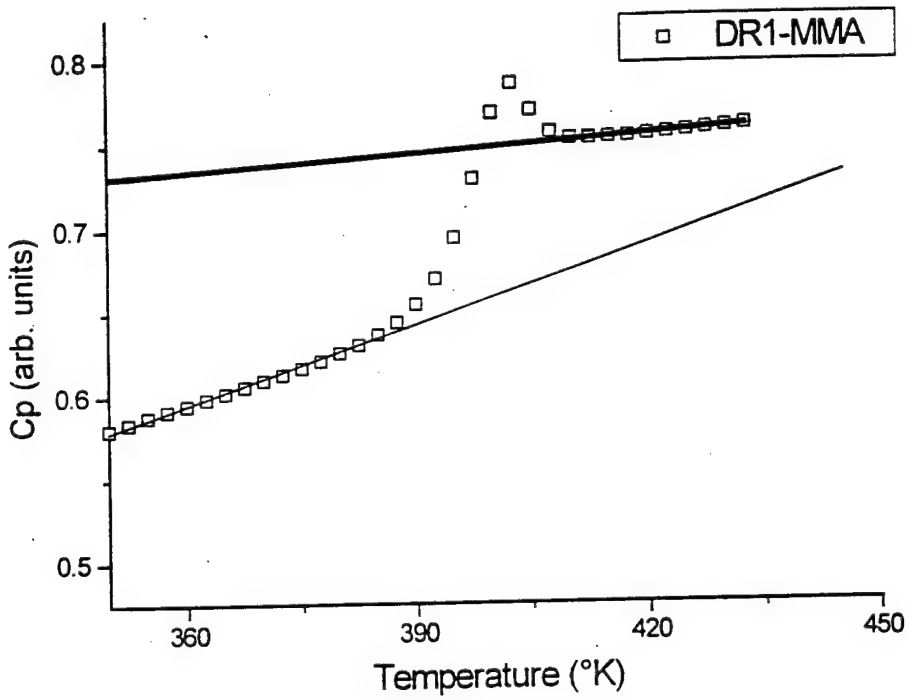
DR1-MMA
0.8
0.7
0.6
0.5
Cp (arb. units)
360
390
420
450
Temperature (°K)

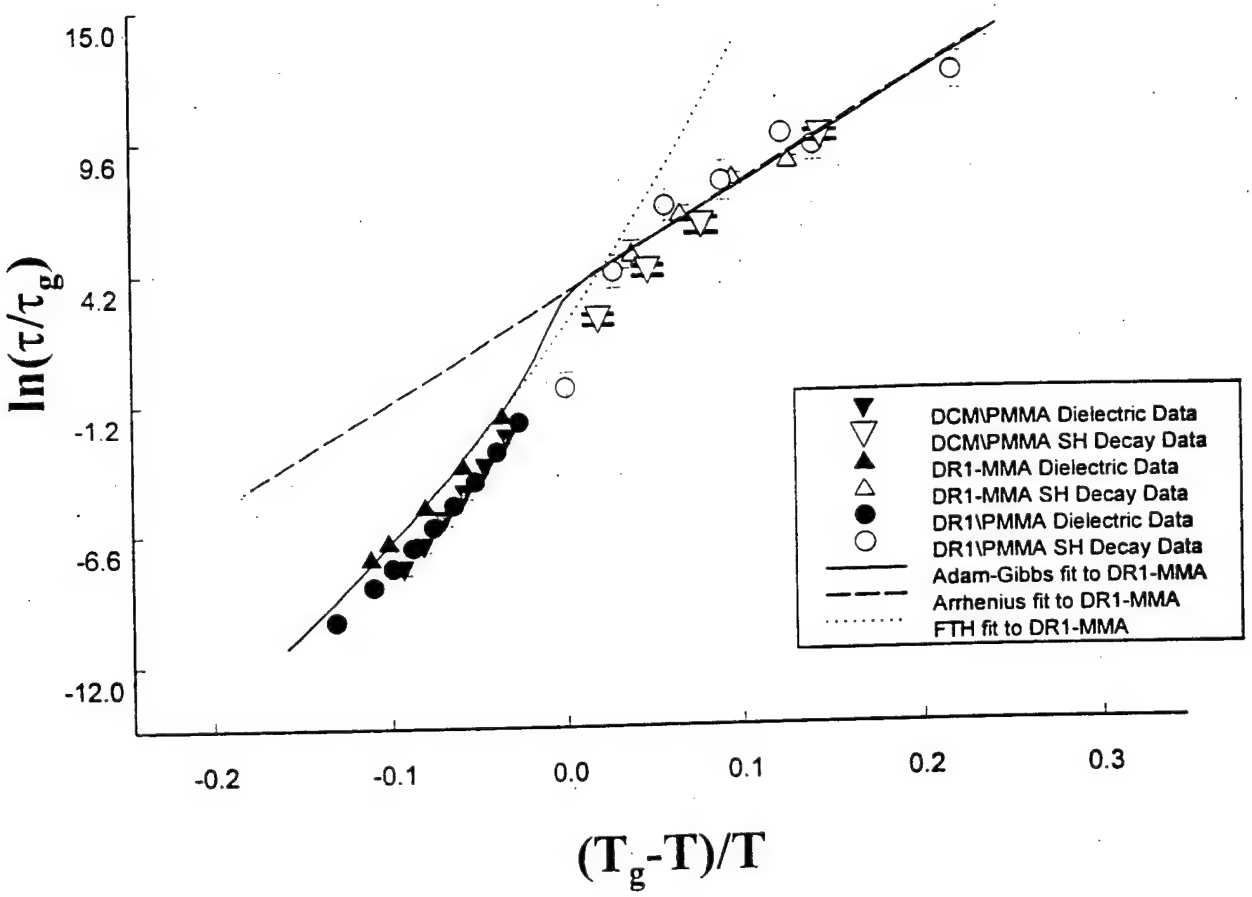
15.0
9.6
4.2
-1.2
-6.6
-12.0
ln(τ/τg)
-0.2
-0.1
0.0
0.1
0.2
0.3
(Tg-T)/T
DCM\PMMA Dielectric Data
DCM\PMMA SH Decay Data
DR1-MMA Dielectric Data
DR1-MMA SH Decay Data
DR1\PMMA Dielectric Data
DR1\PMMA SH Decay Data
Adam-Gibbs fit to DR1-MMA
Arrhenius fit to DR1-MMA
FTH fit to DR1-MMA

Appendix 2

Cross-Linked Polyimides for Integrated Optics
K.D. Singer et al.

SPIE Proceedings manuscript from a critical reviews session of the July 1997 meeting
In press, to appear Fall, 1997

Cross-linked Polyimides for Integrated Optics

K.D. Singer

Case Western Reserve University Department of Physics, Cleveland, OH 44106-7079

T.C. Kowalczyk†and H.D. Nguyen

NASA Lewis Research Center, 21000 Brookpark Rd., Cleveland, OH 44135
†Present Address: Deacon Research, 2440 Embarcadero Way, Palo Alto, CA 94303

A.J. Beuhler‡and D.A. Wargowski

Amoco Chemical Co., Amoco Research Center, Naperville, IL 60566
‡Present Address: Motorola Corp., Northbrook, IL 60062

ABSTRACT

We have investigated crosslinkable polyimides for both passive and active electro-optic devices. These fluorinated polyimides are soluble in the imidized form and are both thermally and photo-crosslinkable leading to easy processability into waveguide structures and the possibility of stable electro-optic properties. We have fabricated channel and slab waveguides and investigated the mechanism of optical propagation loss using photothermal deflection spectroscopy and waveguide loss spectroscopy, and found the losses to arise from residual absorption due to the formation of charge transfer states. The absorption is inhibited by fluorination yielding propagation losses as low as 0.4 dB/cm in the near infrared. Channel waveguides formed by a simple wet etch process are observed to have no excess loss over slab structures. We have produced electro-optic polymers by doping with the nonlinear optical chromophores, DCM and DADC; and a process of concurrent poling and thermal crosslinking. Multilayer structures have been investigated and poling fields optimized in the active layer by doping the cladding with an anti-static agent.

1. INTRODUCTION

Organic polymers have received much attention as promising materials for integrated optics because they have low optical losses and are compatible with existing photolithographic fabrication procedures. [1] They can be

formed into both passive and active device structures and are easily integrated with electronic circuits since they can be easily spin deposited onto semiconductor substrates. Furthermore, polymers can be cast into multilayers containing channels, ribs, and other routing devices. In addition, for active applications, their low dielectric constant implies applicability to microwave frequency electro-optic devices. [2,3] Much effort in improving electro-optic polymers is currently being focused on optimizing the molecular optical nonlinearity, the $\mu\beta$ product, and in increasing the thermal stability of the electro-optic coefficient.

The instability of the electro-optic coefficient arises from the electric field poling process used to induce the polar order necessary for attaining the Pockels effect. The induced polar order is not in thermodynamic equilibrium due to the glassy nature of the polymer, and thus orientational relaxation occurs. Current approaches to optimizing stability has included the use of main chain chromophores, side chain chromophores, and crosslinked systems. [4–6] These materials have higher glass transition temperatures and reduced orientational mobility as compared to their guest-host analogs and consequently reduced chromophore relaxation. Guest-host polyimides have been employed to optimize thermal stability of induced orientation while maintaining functionality. Polyimides are well known in the electronics industry for their thermal integrity, resistance to organic solvents, and compatibility with silicon fabrication processes. Initial guest-host polyimides required imidization and densification at high temperature requiring that dopant molecules have high thermal decomposition temperatures. [7,8] In studies where the chromophores did not thermally decompose, sublimation and plasticization occurred. [9,10] Alternatives to high temperature imidization have been developed and include chemical imidization and preimidized soluble polyimides. [11,12] In these cases, densification for extended periods of time was necessary to minimize the free volume around the chromophore and reduce thermal relaxation of induced orientation. [13] More recently, side-chain polyimides have been developed. [14–16] These materials imidize at temperatures below the thermal decomposition temperatures of most chromophores and have demonstrated excellent thermal stability of induced orientation for over 200 hours at elevated temperatures. The additional orientational stability is presumably due to the hindered rotational motion of the large polyimide chains.

We review here our approach to the development of device-quality electro-optic materials using perfluorinated preimidized fully aromatic polyimides. Preimidization makes processing doped polymer systems more flexible, by making functionalizing easier while allowing spin coating of soluble fully-imidized polymers. Fluorination increases solubility while decreasing optical loss and refractive index. Fully aromatic polymers allow for the

best high temperature properties. We found that by introducing alkylated aromatic crosslinking groups which can be photo- or thermally activated, optical losses were greatly reduced, and high quality waveguides could be fabricated. The photo-crosslinking also permits a simple liquid etch process to define waveguides, and provides a chemical hook to which chromophores may be covalently attached to these polymers. We present our efforts to incorporate this material system in microwave frequency integrated optic devices.

2. POLYMER WAVEGUIDES

Waveguiding in passive polymer structures were studied. Single-layer guides on glass or SiO_2 substrates were studied to determine the intrinsic optical properties such as refractive index and loss. Polymer core-cladding structures were also fabricated in order to evaluate materials in passive device geometries.

We studied optical losses in polyimide waveguides in order to understand the mechanisms responsible for losses and to develop new polyimides with lower losses. [17,18] Low loss waveguides could be produced by attaching perfluoro (CF_3) groups to the polymer backbone. The addition of these groups decreases absorption in the visible wavelengths by reducing charge transfer and creating polymer deformation.

Polyimides were synthesized with increasing amounts of fluorination as shown in Fig. 1 (in order of increasing fluorination). The details of synthesis have been reported elsewhere. [19] Refractive indices and optical losses were measured by waveguide techniques as well as by photothermal deflection spectroscopy. [17,18] Refractive indices were observed to decrease with increasing fluorination. The low refractive index results from its low density due to the presence of alkylated aromatic crosslinking groups [20] and a high degree of fluorination. It was determined that propagation losses in waveguides was mainly due to absorption arising from charge transfer absorption bands in the polyimide. Losses were observed to decrease with increasing fluorination. Because of the low losses and fabrication advantages of cross-linkable materials, Ultradel 9020D and 9120D were selected for further studies of both active and passive waveguides. Table 1 contains physical and optical properties of Ultradel 9020D and 9120D. It is seen from the table that these materials are indeed promising materials for both passive and active applications. They exhibit both low dielectric and optical losses, are thermally stable, and possess useful coefficients of thermal expansion. In ad-

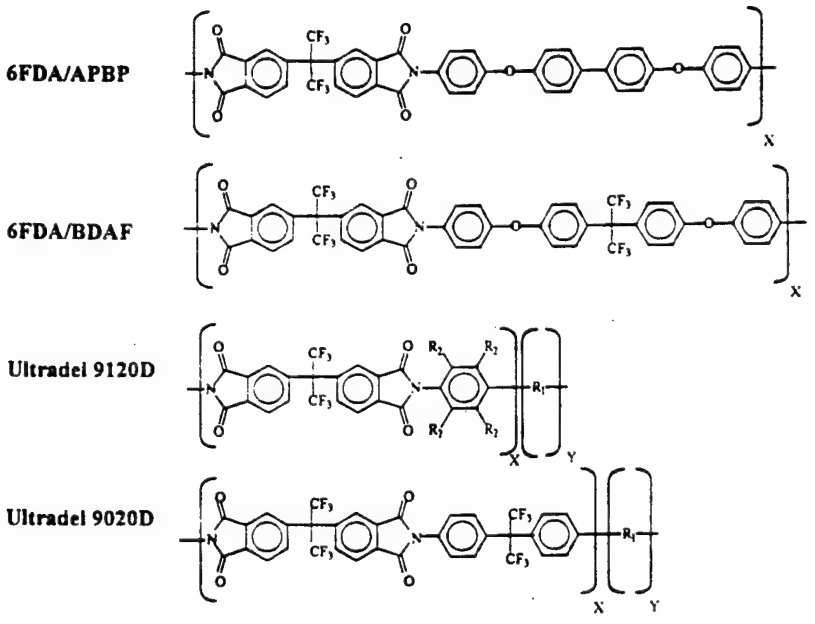

FIG. 1. Chemical structures of polyimides used in this study are listed in order of increasing fluorination. Ultradel 9020D and 9120D are crosslinkable polyimides that can be used as a core cladding pair. (R_1 = alkylated aromatic crosslinking group as described in reference 18)

Property	Ultradel 9020D	Ultradel 9120D
Refractive Index @		
633nm	TE=1.5486, TM=1.5224	TE=1.5624,TM=1.5287
833nm	-	TE=1.5504,TM=1.5213
1064nm	TE=1.5311, TM=1.5073	TE=1.5467, TM=1.5162
1310nm	TE=1.5285, TM=1.5040	TE=1.5364, TM=1.5073
1550nm	-	TE=1.5337, TM=1.5047
Absorption Coefficient @	dB/cm	dB/cm
633nm	1.29	1.04
830nm	0.34	0.13
1064nm	0.26	0.09
1300nm	0.43	0.34
1550nm	0.99	1.21
Tg	390°C	420°C
TGA, 1% wght. loss		
Nitrogen	507°C	450°C
Air	440°C	457°C
Moisture Uptake, @ 100% R.H.	3.0%	3.9%
Dielectric Constant, 1MHz	2.6	2.8
Dissipation Factor, 1mhz	0.005	0.004
Tensile Modulus	GPa	Gpa
40°C	1.467	2.844
100°C	1.398	2.796
250°C	0.980	1.839
-40°C	1.442	2.487
CTE	ppm/°C	ppm/°C
25-50°C	58.1	56.8
25-100°C	57.6	55.3
25-200°C	59.0	54.4
25-300°C	61.3	55.2
CTE (Bellcore)	ppm/°C	ppm/°C
-40 to 0°C	34.2	42.9
-40 to +40°C	44.0	50.2
-40 to +85°C	48.8	52.1

Table 1. Physical and optical properties of Ultradel 9020D and 9120D. (TGA=thermal gravimetric analysis; CTE=coefficient of thermal expansion)

dition, the refractive indices suggest that a core-clad structures with 9120D core and 9020D cladding would be possible to make.

Clad passive waveguide structures were fabricated using a wet etch process which we will describe in a later section. Structures, as shown Fig. 2, with Ultradel 9120D as a core and 9020D as a cladding were made and waveguide losses were measured. Losses were also observed to be highly cure dependent as shown in that figure. At temperatures greater than 350° C, increased losses are due to polyimide decomposition. However, as seen in the figure, losses in the core-clad waveguides as low a 0.4 dB/cm were attained. In addition, these losses were as low as observed in single layer waveguides, indicating that the waveguide fabrication process introduced no additional losses. [17]

Nonlinear optically active materials are made by mixing nonlinear optical chromophores into the host material. The introduction of nonlinear chromophores may introduce additional losses in the form of scattering sites and absorption tails which can be further enhanced upon poling. [21] Fig. 3 depicts the structure of our nonlinear optical dopants, DCM [22,23] and DADC [24]. In both cases significant losses are introduced by the chromophore. Fig. 4 depicts the additional waveguide losses associated with incorporation of the nonlinear optical dye. This loss arises from absorption tails induced in the materials, probably due to the formation of charge transfer complexes between the dye and polymer. The fully aromatic nature of the polymer likely contributes to this. The formation of these absorption tails may be inhibited by using structures less likely to form charge transfer complexes.

3. ELECTRO-OPTIC PROPERTIES

Electro-optic polymers are produced by doping the polyimide with nonlinear linear optical chromophores and followed by electric field poling. [25] Ultradel 9020D was doped with thermally stable chromophores, DCM and DADC, and electric field-poled to impart an electro-optic response. DCM is a highly nonlinear chromophore with low molecular weight that is photo-bleachable in the UV. [22] Using DCM as a dopant, we can obtain large nonlinearities because high number densities are possible. While DCM's decomposition temperature remains above the processing temperature of Ultradel 9020D, other researchers have reported sublimation at temperatures as low as 220° C. [10] DADC, a chromophore developed for high temperature electro-optic applications, has a high nonlinearity, high molec-

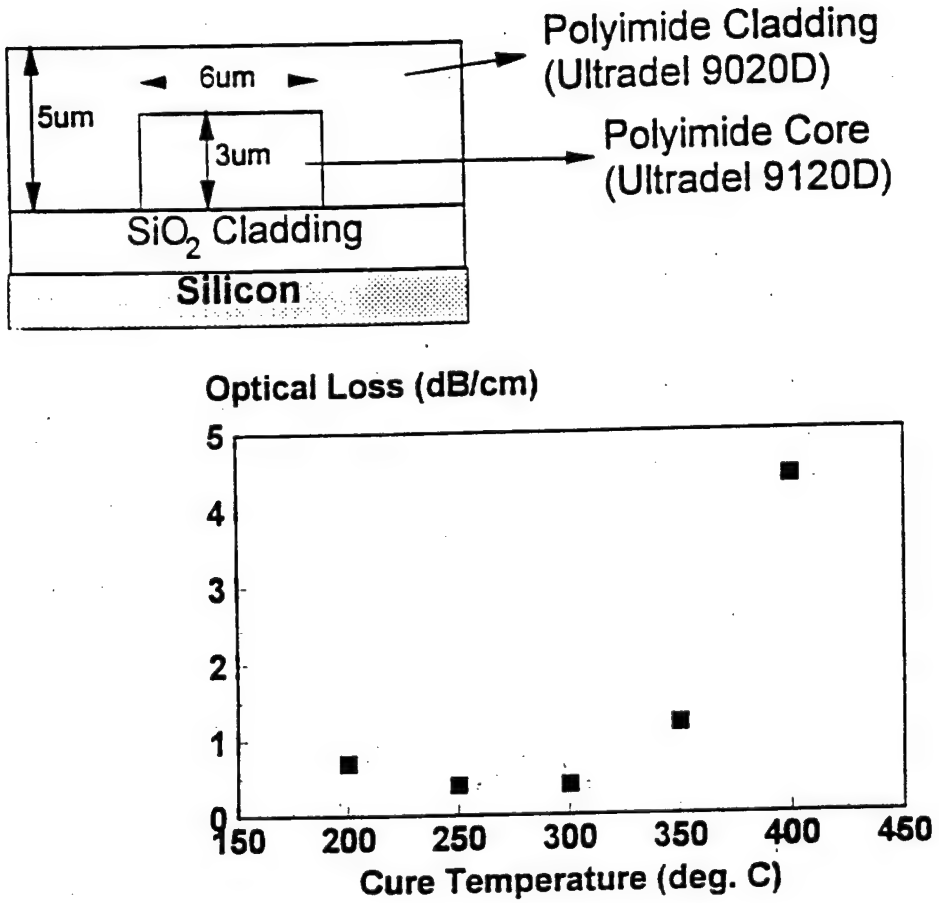

FIG. 2. Core-clad waveguide structure. Waveguide loss data at $\lambda = 800$ nm plotted as a function of curing temperature. Thermal crosslinking occurs near 200^0C.

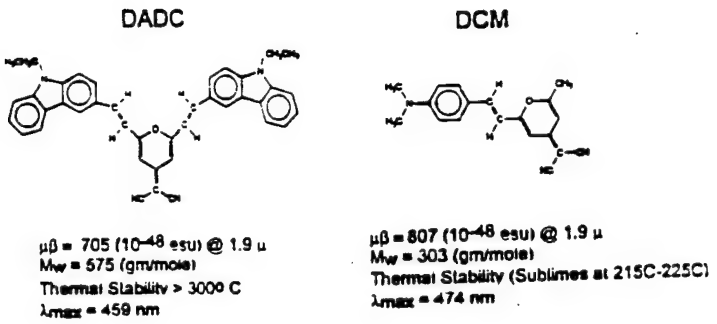

FIG. 3. Chemical structures and properties of thermally stable high temperature chromophores DADC and DCM.

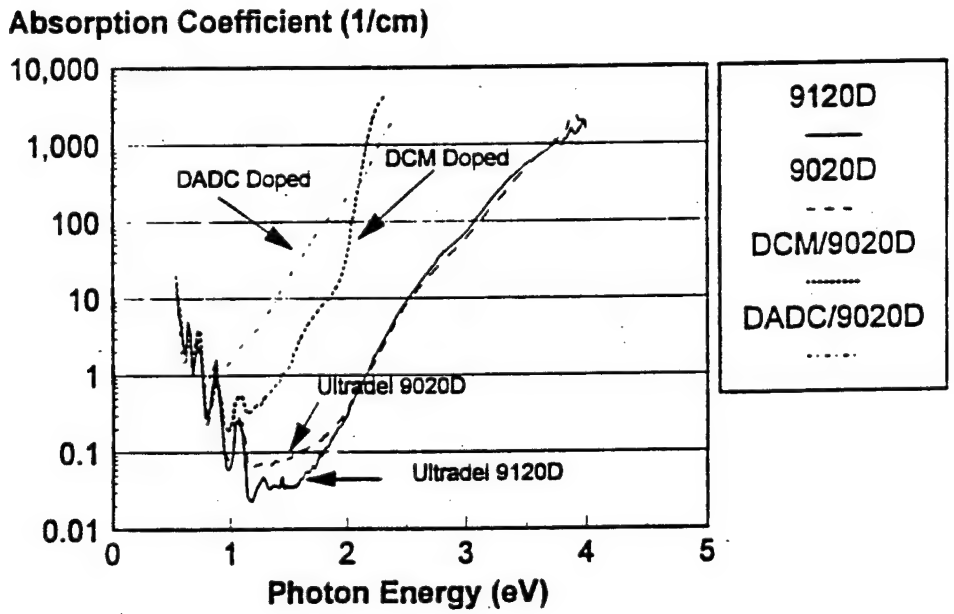

FIG. 4. PDS spectra showing the absorptive losses for Ultradel 9020D, Ultradel 9120D, DCM/Ultradel 9020D, and DADC/Ultradel 9020D. Chromophore loading is 17% by weight fraction. Curing temperature for these samples were 300 C, 300C, 175 C and 300 C, respectively

	DCM/Ultradel 9020D				DADC/Ultradel 9020D		
$T_{poling}(^{\circ}C)$	175	195	215	235	175	225	275
$r_{33}(0)$(a.u.)	0.74	1.0	0.97	0.61	1.0	1.0	0.96
$r_{33}(t)$(a.u.)	0.23	0.49	0.48	0.27	0.58	0.96	0.92
$r_{33}(t)/r_{33}(0)$	0.31	0.49	0.49	0.44	0.58	0.96	0.96

Table 2. Dependence of the electro-optic coefficient on poling temperature. The maximum electro-optic coefficient for DCM and DADC immediately after poling is scaled to unity.

ular weight, and is also photo-bleachable in the UV. [24] Using DADC we expect lower nonlinearities than DCM because of lower number densities at a given weight fraction. DADC's larger structure eliminates sublimation even at temperatures as high as 400° C. TGA (thermogravimetric analysis) experiments have shown only a 2% weight loss in nitrogen at temperatures as high as 400° C. [22]

The optimum poling temperature was determined by comparing samples poled with the same field at varying temperatures. Orientation and relaxation were probed by measuring the in-plane electro-optic coefficient at 800 nm with a Mach-Zehnder interferometer. [26] The electro-optic coefficient was measured immediately after poling for both sets of samples. Afterwards, the samples were placed into an oven at 125° C for approximately 50 hours, and the electro-optic coefficient was remeasured. Table 2 shows the results for both DADC and DCM. For DADC the electro-optic coefficient before aging is constant with temperature. After thermal aging, the sample poled below 200° C decayed while those above 200° C remained stable. This indicates that crosslinking occurs just above 200° C.

Table 2 shows that the ratio. $r_{33}(t)/r_{33}(0)$, for DCM is fairly constant for temperatures above 200° C. At higher temperatures, $r_{33}(0)$ was lower. We attribute this to sublimation of the chromophore at elevated temperatures. Interestingly, the chromophore retention depends on the initial concentration which may be evidence of the chromophore plasticizing the polymer. The enhanced orientational decay of DCM at all temperatures may be attributed to plasticizing of the polyimide. [12]

The equation relating the electro-optic coefficient to its microscopic

parameters at a particular wavelength is given by [25],

$$r_{ij,k}(-\omega;\omega,0) = \frac{-4N\beta_{zzz}L_3(p)}{n_\omega^4}\frac{f^\omega f^\omega f^o}{f^{2\omega'}f^{\omega'}f^{\omega'}}\frac{(3\omega_o^2-\omega^2)(\omega_o^2-\omega'^2)(\omega_o^2-4\omega'^2)}{3\omega_o^2(\omega_o^2-\omega^2)^2} \tag{1}$$

$$p = f^o\frac{\mu E_p}{k_B T_p} \tag{2}$$

where N is the chromophore number density, β_{zzz} is the second order microscopic susceptibility, $L_3(p)$ is the third-order Langevin function, μ is the dipole moment, E_p is the poling field, k_B is the Boltzmann constant, T_p is the poling temperature, f^o is the Onsager local field factor for the static poling field, $f^\omega f^{2\omega'} f^{\omega'}$ are the Lorenz-Lorentz local field factors at optical frequencies, ω' and $2\omega'$ are the frequencies used in the second harmonic generation experiment, ω_o and ω are the resonance and electro-optic experiment frequencies, respectively. Fig. 5 shows the agreement between Eq. 1 and experiment indicating full poling and verifies the electronic nature of the electro-optic effect. The solid lines define the $(+/-)15\%$ error in the measurement of $\mu\beta$. The slight offset of electro-optic coefficient at larger poling fields is probably due to increased birefringence with increasing poling fields.

4. THREE-LAYER ACTIVE WAVEGUIDES

Nonlinear optical materials must be formed into channel, slab, or rib waveguides for integrated optical applications. The resistance of crosslinked Ultradel 9020D to organic solvents makes it a suitable material for layered devices. We formed three-layer slab waveguides by spinning and curing successive layers of Ultradel 9020D on ITO-coated glass. The layered structures consisted of DCM- and DADC-doped Ultradel 9020D cores surrounded by neat Ultradel 9020D cladding layers. To obtain noncentrosymmetric ordering as well as large poling field induced nonlinearities in three-layered devices, it is essential for the cladding layers to be more conductive than the core layer so that the voltage drop, and hence the poling field, across the active layer is as large as possible. Direct measurements of the poling field are not possible in three-layer samples because the voltage splitting between core and cladding layers is unknown. The effective poling field can be determined indirectly by measuring the macroscopic susceptibility's dependence on the externally applied field and comparing to theory. The macroscopic

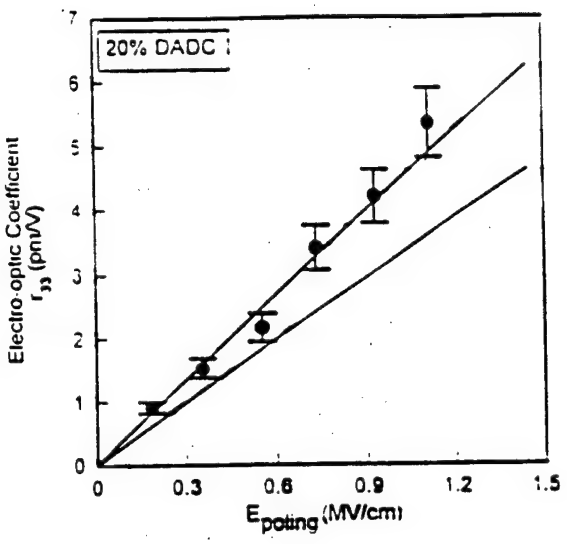

FIG. 5. Electric field dependence of electro-optic coefficient for 17% DADC by weight fraction. Solid lines represent (+/-)15% uncertainty in $\mu\beta$ values as input to the theory. Data points are from electro-optic experiment where $r_{33} = 3r_{13}$ was assumed.

susceptibility was measured using the Rotational Maker Fringe (RMF) technique as a function of poling field for single- and three-layer samples. [27] Gold electrodes were sputtered onto the samples for contact poling. After contact poling, the gold was removed and the RMF experiment was performed. Measurements were made using the 2nd Stokes line ($\lambda = 1.367\mu$) of a hydrogen-filled Raman cell that was pumped by the output of a Nd:YAG pumped pulsed dye laser. The measured second harmonic coefficients in the single layer films for both dopants was found to agree with an oriented gas model similar to Eq. 1. The agreement between theory and experiment shows that the oriented gas model adequately describes the poling induced ordering in polyimide materials.

The data for three-layer samples appear in Fig. 6 for DCM- and DADC-doped samples. The two sets of data points on the graphs represent different methods of calculating the poling field across the active layer. The open data points assume the resistivities of all three layers are identical and the resulting poling field is obtained by dividing the applied voltage by the total thickness. The shaded data points use a scaling factor to fit the experimental data to the theoretical prediction of Eq. 3 with the poling field as an adjustable parameter. If we assume the three-layer sample can be modeled by resistors in series, then the scaling factor can be related to the cladding and core resistances by the following equation,

$$V_{eff} = \frac{R_{core}}{R_{core} + 2R_{cladding}} V_{applied} \quad (3)$$

where R_{core} and $R_{cladding}$ are the resistances of the core and cladding layers, and V_{eff} and $V_{applied}$ are the effective and applied poling voltages. [28] The open data points show the inadequacy of assuming equal resistivities to determine the poling field across the active layer. For DCM triple-layers, a value of U=0.4 is used for the best fit adjustable parameter, while for DADC triple-layers, a value of 0.11 is obtained. Conductivity of thin single-layer films was used to independently calculate the effective poling field. The conductivity and thickness of DADC triple-layers poled at 250° C predicts a correction factor of 0.1 in excellent agreement with the best fit. Thus, the voltage division model appears valid. For DCM triple-layers poled at 225° C Eq. 3 predicts an effective poling field an order of magnitude smaller than the best fit adjustable parameter. This discrepancy may be due to migration of DCM into the cladding layers which lowers the conductivity of the core layer while increasing the conductivity of the cladding layers. This migration is consistent with the sublimation observed in single-layer films. The optimization of poling requires that the conductivity of the cladding be much larger than the core to maximize the electric field in the active layer.

To this end, we have incorporated ionic dopant [29] consisting of a graft polymer incorporating a quaternary ammonium salt (used as an anti-static agent) into the cladding layers to increase the conductivity. A polymeric salt distributes throughout the cladding layers in contrast to small molecule salt which would reside at the surface. Measurements of the imaginary part of the dielectric constant which is proportional to the conductivity are shown in Fig. 7 as a function of concentration. It is seen at low concentrations that the conductivity is nearly linear, but becomes exponential at higher concentrations. When the axis is scaled to the measured conductivities of the undoped polyimide and the DADC doped polyimides, the conductivity of the core layer is shown as a dotted line. We expect that the ionic doped layer at 18% loading will have the requisite conductivity to amplify the field in the core substantially. Fig. 8 depicts the second harmonic coefficient for a three layer film consisting of 18% ionic doped cladding and a core containing 15% DADC by weight. The line is a fit to the oriented gas model. The fit factor is about 0.3 indicating that the field is divided nearly equally between the three layers. This factor is considerably less than the value of 0.5-0.6 we would expect from the conductivity in Fig. 7 though substantially higher than the 0.11 without the ionic dopant. This discrepancy may be due to the decomposition or sublimation of the ionic dopant during the poling process. Refractive index measurements of the doped polymer before and after high temperature processing support this conclusion.

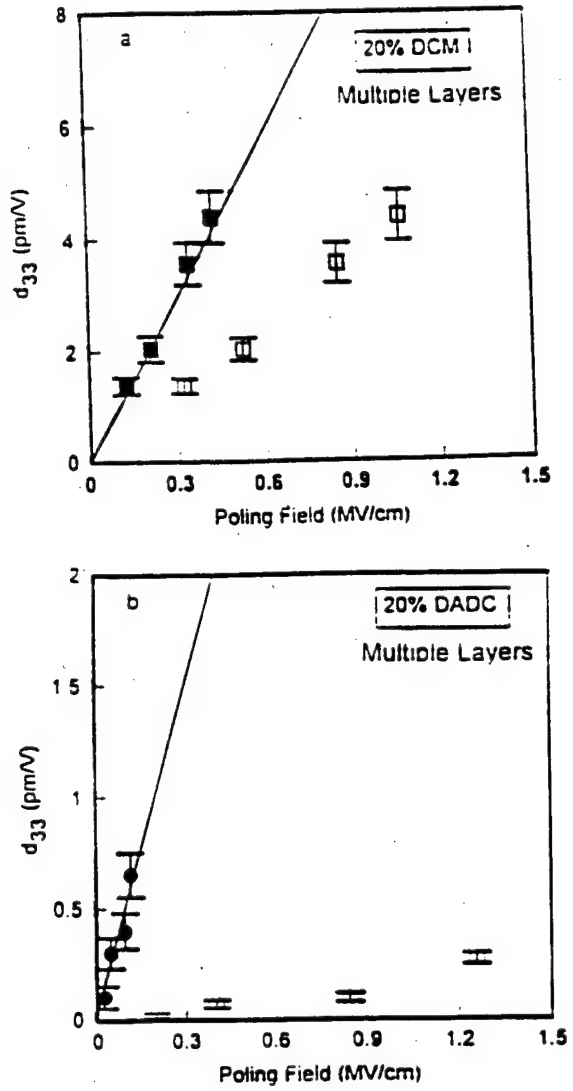

FIG. 6. d_{33} versus poling field for three layer stacks of (a) DCM/Ultradel 9020D and (b) DADC/Ultradel 9020D. Solid lines represents fit to an oriented gas model. Data points are measurements from three-layer samples using the poling field as an adjustable parameter. Best results (shaded data points) are obtained using 0.4 as the best fit parameter for DCM samples and 0.1 for DADC samples. (unshaded data points) assume that resistances of all layers are equal.

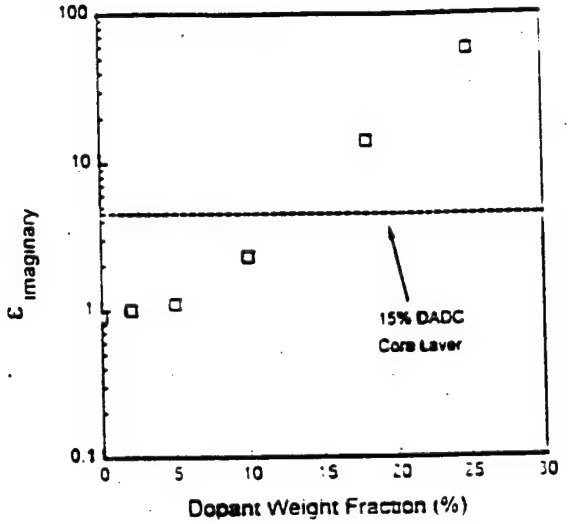

FIG. 7. Imaginary dielectric constant for ionic doped polyimide. The dotted line indicates the approximate core equivalent conductivity.

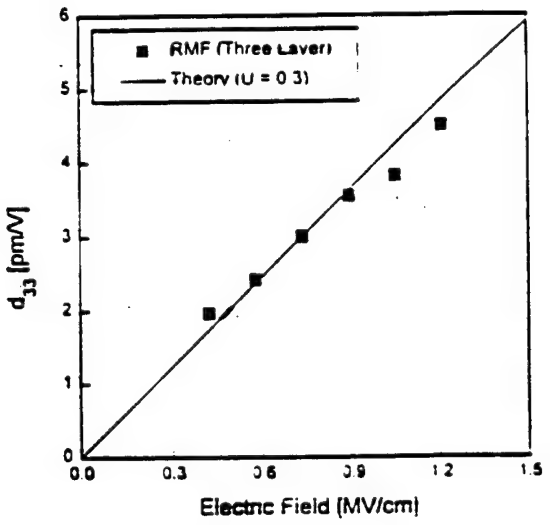

FIG. 8. Three layer second harmonic coefficient data for three layer films with 18% by weight ionic doping in the core and 15% DADC doping in the core. Fit is to an oriented gas model.

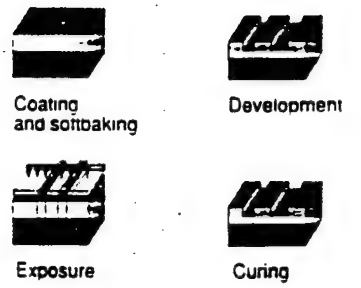

FIG. 9. Processing schematic for fabrication of single mode polyimide waveguides.

5. CHANNEL DEVICE FABRICATION

A processing scheme for creating channel devices has been developed. This process is shown in Fig. 9. The photosensitive polymer is spin-deposited onto a substrate, and soft-cured (below $200°C$) to remove solvent. The polymer is exposed through a photomask leading to photo-crosslinking, and then partially etched with organic solvent developers into a rib or channel pattern. The coating is then post-baked at $300 - 350°C$ to remove residual solvent and to fully crosslink. Either rib or channel waveguides can be produced with this method.

Fig. 10 shows a SEM micrograph of a rib structure fabricated using photosensitive polyimides showing their high quality structure. Channels and ribs 4-5 microns wide have been produced. After post-cure, the films can withstand processes such as metallization, overcoating, thermal cycling, and solvent exposure. Waveguide loss spectroscopy was carried out on three-layer rib waveguides composed of two variations of Ultradel 9020D polymers with appropriate refractive indices. No excess optical loss was introduced by channel waveguide fabrication.

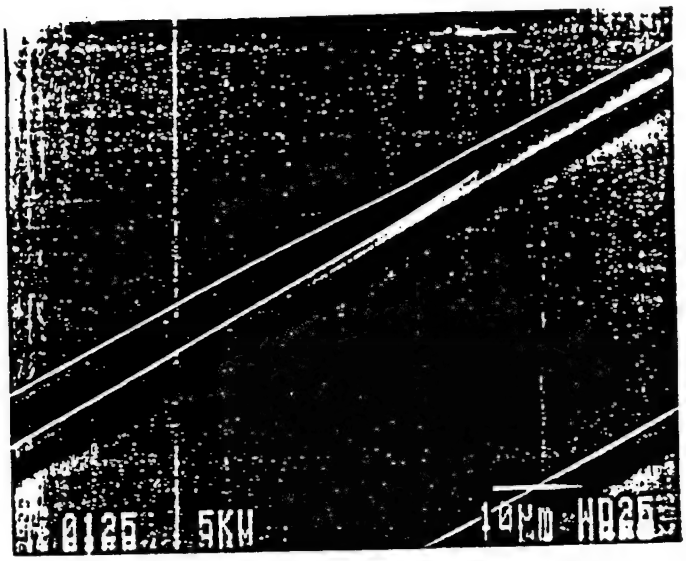

FIG. 10. SEM of a 5.0 μm y-branch waveguide etched in Ultradel 9020D.

6. RF ELECTRODE DESIGN

We describe here electrode design for our polyimide materials similar to that carried out for other polymer systems. [2,30] In the design of high speed modulators, a key factor is the relative velocities of the microwave and optical signals as they propagate down the device. The coupling efficiency between the waves depends on the velocity match between the waves with the upper frequency limit depending on this phase velocity match. Polyimides are well-known for their low dielectric constant; in fact, the microwave dielectric constant and the optical refractive index squared can be very close so that the velocity match is not the limiting factor in such devices. We have designed microstrip electrodes for propagation of microwave frequency signals in a modulator. [31]

The geometry of the microstrip line and the optical waveguide are shown in Figs. 11 and 12 with the microstrip line placed directly over the polymer waveguide. An impedance match taper is also included. To characterize the structure, the microstrip characteristic impedance Z_0, the microstrip propagation constant, $\gamma = \alpha + j\beta$, the length of the coupling region L, the source voltage V_0, and the source and load impedances Z_S and Z_L are required. In the case of this geometry, the total optical phase shift due to the electro-optic effect is given by,

$$\Delta\phi = \delta r(f)\sin(\phi - 2\pi f_m t) \tag{4}$$

where δ is the electro-optic phase shift given by

$$\delta = \frac{\pi n^3 r V_0 \Gamma L}{\lambda H} \tag{5}$$

with n being the index of refraction. r the electro-optic coefficient, H the device thickness, Γ the electrical-optical overlap parameter, λ the optical wavelength, and L the propagation length. The parameter ϕ is the phase delay between the RF and optical wave which will be defined below. The frequency dependent amplitude response is given by,

$$R(f) = 10 \log r(f) + P_{RF} \tag{6}$$

where P_{RF} is the required RF power. and

$$r(f) = \sqrt{\frac{a^2 + b^2}{e^{2\alpha L}(1 - \rho_S \rho_L e^{-2\alpha L})^2((KL)^2 + (\alpha L)^2)^2}}. \tag{7}$$

Here, we have ρ_S and ρ_L the RF source and load reflection coefficients, $K = (2\pi f \Delta n)/c$, with $\Delta n = \sqrt{\epsilon_{eff}} - n$ proportional to the difference in phase velocities between the microwave and optical wave. Finally,

$$\begin{aligned} a = {} & L(K\cos(KL) + \alpha \sin(KL) - Ke^{\alpha L}) \\ & + LT(e^{2\alpha L} K \cos(KL) - e^{2\alpha L} \alpha \sin(KL) - K) \end{aligned} \tag{8}$$

$$\begin{aligned} b = {} & L(K\sin(KL) - \alpha \cos(KL) + \alpha e^{\alpha L}) \\ & + LT(e^{2\alpha L} K \sin(KL) + e^{2\alpha L} \alpha \cos(KL) - \alpha) \end{aligned} \tag{9}$$

and

$$T = \rho_L \rho_S e^{-2\alpha L}. \tag{10}$$

The phase delay is $\phi = \tan^{-1}(a/b)$. Because Δn is so small in polyimides, it the attenuations and reflections that limit the 3 dB bandwidth. The responsivity R(f) was calculated for a number of heights, H, as a function of frequency and shown in Fig. 13. In generating Fig. 13, a 50 ohm impedance at the input and output ports, a width of 15 μm, a length of 1.2 cm, dielectric constant = 2.6, tan $\delta = 0.002$, and refractive index of 1.61 were used. Note the 3 dB bandwidth out to 50 GHz. The microstrip fabricated using these parameters predicts an R(f) electro-optic response as shown in Fig. 14. These predictions were made from measured insertion losses. Good agreement is seen with the simulations, and a bandwidth greater than 40 GHz is expected.

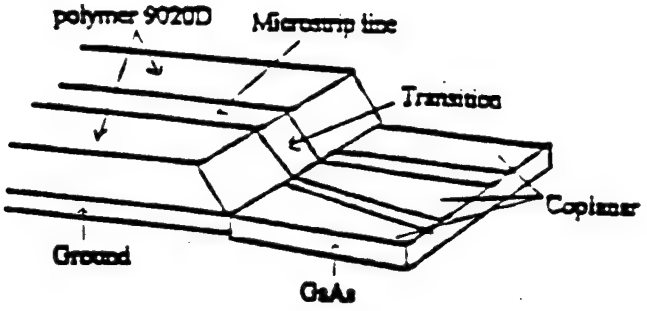

FIG. 11. Section of microstrip-coplanar transition on polyimide waveguide.

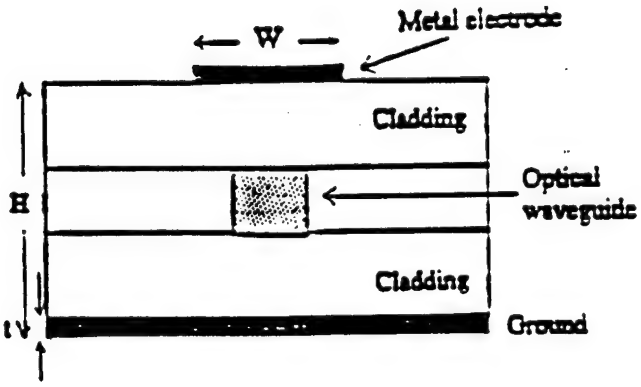

FIG. 12. Cross section of the optical waveguide microstrip device.

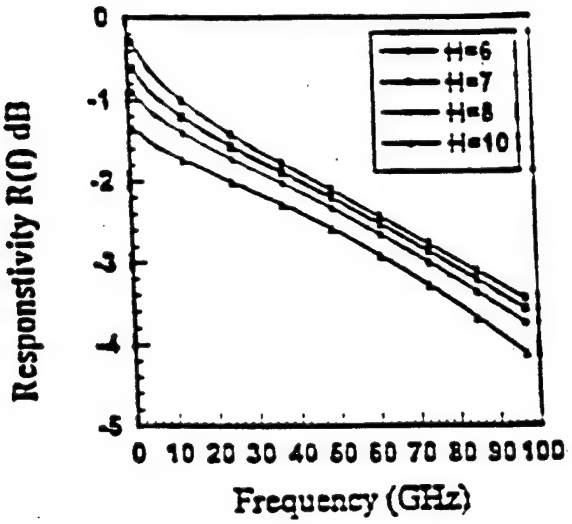

FIG. 13. Calculated modulator amplitude response versus frequency for a microstrip width of 15 μm.

7. CONCLUSIONS

We have described the development of a crosslinkable polyimide material system for integrated optical applications. First, we optimized the optical and waveguide processing properties, and later introduced functionality by guest-host inclusion and electric field poling. From optical waveguide and PDS measurements we determined the primary mechanism for optical waveguide loss in polyimide waveguides is absorption from electronic absorption tails. The measured waveguide loss in Ultradel 9020D of 0.4 dB/cm at 800 nm and predicted losses of 0.4 dB/cm at 1300 nm make these materials excellent candidates for integrated optical applications. Introduction of the active chromophores, DCM and DADC, increased the optical losses as determined by PDS. We believe that these long absorption tails may be a general problem in many electro-optic polymers, but especially so in aromatic ones like those studied here.

We then investigated the electric field poling conditions. The optimum poling temperature was found to be slightly below the sublimation temperature of DCM and well below the thermal decomposition temperature of most thermally stable chromophores. Both guest-host systems display excellent thermal stability of the electric field-induced orientation at room temperature. At elevated temperatures, significant orientational relaxation occurred in DCM-doped samples. The enhanced decay may be attributed

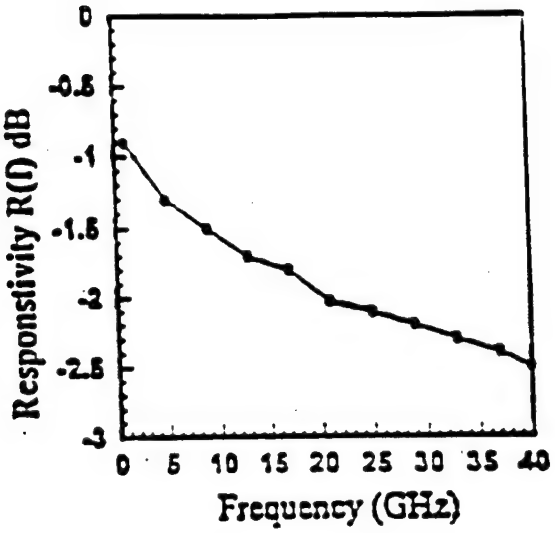

FIG. 14. Responsivity, R(f) of a polymer electro-optic modulator.

to plasticizing of the polyimide and greater rotational mobility of DCM. The DADC-doped polyimide retained 75% of its initial orientation after 200 hours at 125^0 C.

Three-layer samples of doped polyimide showed nonlinearities smaller than comparable single-layer films. The decrease in nonlinearity is attributed to lower poling fields due to voltage division across the three-layer sample and possibly chromophore migration into cladding regions. The voltage splitting can be eliminated by substituting existing cladding layers with more conductive cladding layers as we observed with an ionic dopant in the cladding layers.

We have also described a simple waveguide processing procedure for forming channel and rib structures which takes advantage of the photocrosslinking nature of polyimide materials and does not introduce excess optical losses. We have also described the fabrication of modulating electrodes with a predicted frequency response to at least 40GHz. We believe that this material system is an excellent candidate for active and passive integrated optical applications. Further refinement in processing and refractive index control are all that is necessary for passive applications. For active applications, the identification of suitable chromophores which do not introduce absorption is necessary. Covalent attachment of active chromophores to crosslinking sites should be straightforward, and would lead to vastly improved performance regarding optical nonlinearity and stability.

8. ACKNOWLEDGEMENTS

Partial support for this work was provided by AFOSR under grant # 49620-93-1-0202. The authors are grateful to Drs. C. Seager, P. Cahill, and C. Sullivan of Sandia Laboratories for photothermal deflection spectroscopy measurements. The authors also wish to thank S. Ermer (Lockheed-Martin Corp.) for supplying DADC, C. Allen (Amoco) for her technical assistance, and Dr. S. Aramaki of Mitsubishi Chemical for providing the V-SQ antistatic agent.

REFERENCES

[1] *Polymers for Lightwave and Integrated Optics*, L. A. Hornak, ed. (Marcel Dekker, New York,1992).

[2] W.S. Wang, D.T. Chen, H.R. Fetterman, Y.Q. Shi, W.H. Steier, L.R. Dalton, and P.M.D. Chow, *Applied Physics Letters* **67**, 1806 (1995).

[3] Y.Q. Shi, W.S. Wang, J.H. Bechtel, A.T. Chen, S. Garner, S. Kalluri, W.H. Steier, D.T. Chen, H.R. Fetterman, L.R. Dalton, and L.P. Yu, *IEEE J. Sel. Top. Quant. Electron.* **2**, 289 (1996).

[4] D.M. Burland, R.D. Miller, and C.A. Walsh, *Chem. Reviews* **94**, 31 (1994).

[5] P.M. Ranon, Y. Shi, H Steier, C. Xu, B. Wu, L.R. Dalton, Appl. Phys. Lett. **62**, 2605 (1993).

[6] B. Wu, C. Xu, L.R. Dalton, S. Kalluri, Y. Shi, and W. H. Steier, in MRS Proc., A.F. Garito, A. Jen, C. Lee, and L.R. Dalton, ed., Materials Research Society, Pittsburgh, **328**, 529 (1994).

[7] J.W. Wu, J.F. Valley, S. Ermer, E.S. Binkley, J.T. Kenney, G.F. Lipscomb, and R. Lytel, Appl. Phys. Lett. **58**, 225 (1991).

[8] J.W. Wu, E.S. Binkley, J.T. Kenney, R. Lytel, and A.F. Garito, J. Appl. Phys. **69**, 7366 (1991).

[9] J.F. Valley, J.W. Wu, S. Ermer, M. Stiller, E.S. Binkley, J.T. Kenney, G.F. Lipscomb, and R. Lytel, Appl. Phys. Lett. **60**, 160 (1992).

[10] H.H. Fujimoto, S. Das, J.F. Valley, M. Stiller, L. Dries, D. Girton, T. Van Eck, S. Ermer, E.S. Binkley, J.C. Nurse, and J.T. Kenney, in MRS Proc., A.F. Garito, A. Jen, C. Lee, and L.R. Dalton, ed., Materials Research Society, Pittsburgh, **328**, 553 (1994).

[11] J.W. Wu, J.F. Valley, S. Ermer, E.S. Binkley, J.T. Kenney, and R. Lytel, Appl. Phys. Lett. **59**, 2213 (1991).

[12] S.F. Hubbard, K.D. Singer, F. Li, S.Z.D. Cheng, and F.W. Harris, Appl. Phys. Lett. **65**, 265 (1994).

[13] K.Y. Wong and A.K.Y. Jen, J. Appl. Phys. **75**, 3308 (1994).

[14] B. Zysset, M. Ahlheim, M. Stahelin, F. Lehr, P. Pretre, P. Kaatz, and P. Gunter, Proc. SPIE **2025**, 70 (1993).

[15] W. Sotoyama, S. Tatsuura, and T. Yoshimura, Appl. Phys. Lett. **64**, 2197 (1994).

[16] D. Yu, A. Gharavi, and L. Yu, Appl. Phys. Lett. **66**, 1050 (1995).

[17] T.C. Kowalczyk, T.Z. Kosc, K.D. Singer, A.J. Beuhler, D.A. Wargowski, P.A. Cahill, C.H. Seager, and M.B. Meinhardt, "Crosslinked Polyimides for Integrated Optics", in *Polymers for Second-order Nonlinear Optics*, G.A. Lindsay and K.D. Singer eds. (ACS Symp. Ser. 601 , 1995) pp. 381-400.

[18] T.C. Kowalczyk, T.Z. Kosc, K.D. Singer, P.A. Cahill, C.H. Seager, M.B. Meinhardt, A. Beuhler, and D.A. Wargowski, J. Appl. Phys. **76** 2505 (1994).

[19] A. Beuhler, D.A. Wargowski, T.C. Kowalczyk, K.D. Singer, Proc. SPIE **1849**, 92 (1993).
[20] Allyson J. Beuhler and David A. Wargowski, "Photodefinable Optical Waveguides", U.S. Patent No. 5,317,082 (May, 1994)
[21] C.C. Teng, M.A. Mortazavi, and G.K. Boudoughian, Appl. Phys. Lett. **66**, 667 (1995).
[22] S. Ermer, J.F. Valley, R. Lytel, G.F. Lipscomb, T.E. Van Eck, D.G. Girton, D.S. Leung, and S.M. Lovejoy, Proc. SPIE **1853**, 183 (1993).
[23] S. Ermer, J.F. Valley, R. Lytel, G.F. Lipscomb, T.E. Van Eck, and D.G. Girton, Appl. Phys. Lett. **61**, 2272 (1992).
[24] S. Ermer, D. Leung, S. Lovejoy, J. Valley, and T.E. Van Eck, in *Organic Thin Films for Photonic Applications Technical Digest*, 1993 Vol. 17 (Optical Society of America, Washington, D.C., 1993) pp. 70-72.
[25] K.D. Singer, M.G. Kuzyk, and J.E. Sohn, J. Opt. Soc. Am. B **4**, 968 (1987).
[26] K.D. Singer, M.G. Kuzyk, W.R. Holland, J.E. Sohn, S.J. Lalama, R.B. Comizzoli, H.E. Katz, and M.L. Schilling, Appl. Phys. Lett. **53**, 1800 (1988).
[27] K.D. Singer, J.E. Sohn, S.J. Lalama, Appl. Phys. Lett. **49**, 248 (1986).
[28] H.C. Ling, W.R. Holland, and H.M. Gordon, J. Appl. Phys. **70** , 6669 (1991).
[29] "V-SQ Anti-static agent" sold by Mitsubishi Chemical Co.
[30] C.C. Teng, *Appl. Phys. Lett.* **60**, 1538 (1992).
[31] H. Nguyen, G.E. Ponchak, R. Kunath, D. Bohman, and N. Varaljay, *Microwave and Opt. Tech. Lett.* **13**, 90 (1996).

[40] K. L. Ngai, C. T. White, "Frequency Dependence of Dielectric Loss in Condensed Matter", Phys. Rev. B, **20** , 2475-2486 (1979).

[41] L. J. Slater, "Generalised Hypergeometric Functions", Cambridge University Press, Cambridge (1966).

[42] L. J. Slater, "Confluent Hypergeometric Functions", Cambridge University Press, Cambridge (1960).

[43] A. J. Kovacs, J. M. Hutchinson, and J. J. Aklonis, "The Structure of Non-Crystalline Materials", ed, P.H. Gaskell, Taylor and Francis, London (1977).

[44] M. Stähelin, D. M. Burland, M. Ebert, R. D. Miller, B. A. Smith, R. Twieg, W. Volksen, and C. A. Walsh, "Reevaluation of the Thermal-Stability of Optically Nonlinear Polymeric Guest-Host Systems", Appl. Phys. Lett. **61**, 1626-1628 (1992).

[45] J. Ferry, "Viscoelastic Properties of Polymers", Wiley, New York (1961).

[46] M. I. Klinger, "Glassy Disordered System: Topology, Atomic Dynamics, and Localized Electron States", Elsevier Science Publishers, North-Holland (1989).

[47] J. H. Gibbs, and E. A. DiMarzio, "Nature of the Glass Transition and the Glassy State", J. Chem. Phys. **28**, 373-383 (1958).

[48] G. Adam, and J. H. Gibbs, "On the Temperature Dependence of Cooperative Relaxation Properties in Glass-forming Liquids", J. Chem. Phys. **43**, 139-146 (1965).

[49] G. W. Scherer, "Use of the Adam-Gibbs Equation in the Analysis of Structural Relaxation", J. Am. Ceram. *Soc.* **67**, 504-511 (1984).

[50] A. Q. Tool, J. Am. Ceram. Soc. **29**, 240 (1946).

[51] 0. S. Narayanaswamy, "A Model of Structural Relaxation in Glass", J. Am. Ceram. Soc. **54**, 491-498 (1971).

[52] I. M. Hodge, and A. R. Berens, "Effects of Annealing and Prior History on Enthalpy Relaxation in Glassy Polymers. 2. Mathematical Modeling", Macromolecules **15**, 762-770 (1982).

[53] C. T. Moynihan, P. B. Macedo, C. J. Montrose, P. K. Gupta, M. A. Debolt, J. F. Dill, B. E. Dom, P. W. Drake, A. J. Easteal, P. B. Witerman, R. P. Moeller, H. Sasabe, and J. A. Wilder, "Structural Relaxation in Vitreous Materials", Ann. N.Y. Acad. Sci., **279**, 15-35 (1976).

[54] M. A. DeBolt, A. J. Easteal, P. B. Macedo, and C. T. Moynihan, J. Am. Ceram. Soc. **59**, 16-21 (1976).

[55] J. D. Ferry, "Viscoelastic Properties of Polymers", 3rd Ed., J. Wiley & Sons, New York (1980).

[56] Purchased from IBM Almaden Research Center- San Jose, CA.

[57] J.A. Cline, W.N. Herman, "Chi-electric Relaxation Frequency Domain Chromophore Dynamics in Nonlinear Optical Polymers", Tech. Digest, "Organic Thin Films for Photonic Applications", Opt. Soc. Am., MD39/1-MD39/4 (1995).

[58] K. D. Singer, M. G. Kuzyk, J. E. Sohn, "2nd-Order Nonlinear-Optical Processes in Orientationally Ordered Materials - Relationship Between Molecular and Macroscopic Properties", J. Opt. Soc. Am. B **4**, 968-976 (1987).

[59] G. T. Boyd, C. V. Francis, J. E. Trend, D. A. Ender, "2nd-Harmonic Generation as a Probe of Rotational Mobility in Poled Polymers", J. Opt. Soc. Am. B **8**, 887-894 (1991).

[60] J. W. Wu, "Birefringent and Electrooptic Effects in Poled Polymer-Films - Steady-State and Transient Properties", J. Opt. Soc. Am. B **8**, 142-152 (1991).

[61] N. G. McCrum, B. E. Read, and G. Williams, "Anelastic and Dielectric Relaxation in Polymeric Solids", John Wiley & Sons Ltd., London (1967).

List of Figures

Figure 6. Experimental setup for frequency domain measurements.

Figure 7. Log-log plot of isothermal second harmonic decay in DR1\PMMA at 50 °C.

Figure 8. Log-log plot of isothermal transient current decay exhibiting low frequency dispersion in DR1\PMMA at 50 °C.

Figure 9. Dielectric in phase and out of phase spectra. In column (a), the **in phase** dielectric components are plotted as a function of frequency for DCM\PMMA, DR1\PMMA, and DR1-MMA respectively. In column (b), the **out of phase** or loss components are plotted for DCM\PMMA, DR1\PMMA, and DR1-MMA respectively. In the loss spectra, the α peaks are visibile at lower frequencies while the β peaks are visible at higher frequencies.

Figure 10. Chielectric in phase and out of phase spectra. In column (a), the **in phase** chielectric components are plotted as a function of frequency for DCM\PMMA, DR1\PMMA, and DR1-MMA respectively. In column (b), the **out of phase** or loss components are plotted for DCM\PMMA, DR1\PMMA, and DR1-MMA respectively.

Figure 11. Electric field dependence of chielectric spectra for DCM\PMMA at fixed temperature. In (a) and (b) the in phase and out of phase components of $\chi^{(2)}$ are plotted as a function of frequency for various poling field amplitudes. In (c) and (d) the in phase and out of phase components are scaled to the applied poling field and show that the $\chi^{(2)}$ response is linear in the applied field.

Figure 12. Reduced temperature dependence plot for τ using experimental data from transient current, second harmonic, dielectric, and chielectric measurements on DR1\PMMA.

Figure 13. Temperature dependence of the heat capacity for DR1-MMA after rate cooling at 5 °C/min. The thin line represents the extrapolated heat capacity of the glassy region. C_{pg} while the thick line represents the extrapolated heat capacity of the equilibrium region, C_{pe}.

Figure 14. Reduced temperature dependence plot for τ scaled to τ_g for the three polymer systems. The solid line represents the Adam-Gibbs model based on enthalpy measurements from DR1-MMA. The dashed line represents an Arrhenius fit based on data points below the glass transition, while the dotted line represents Fulcher-Tammann-Hesse or equivalently WLF behavior above the glass transition.

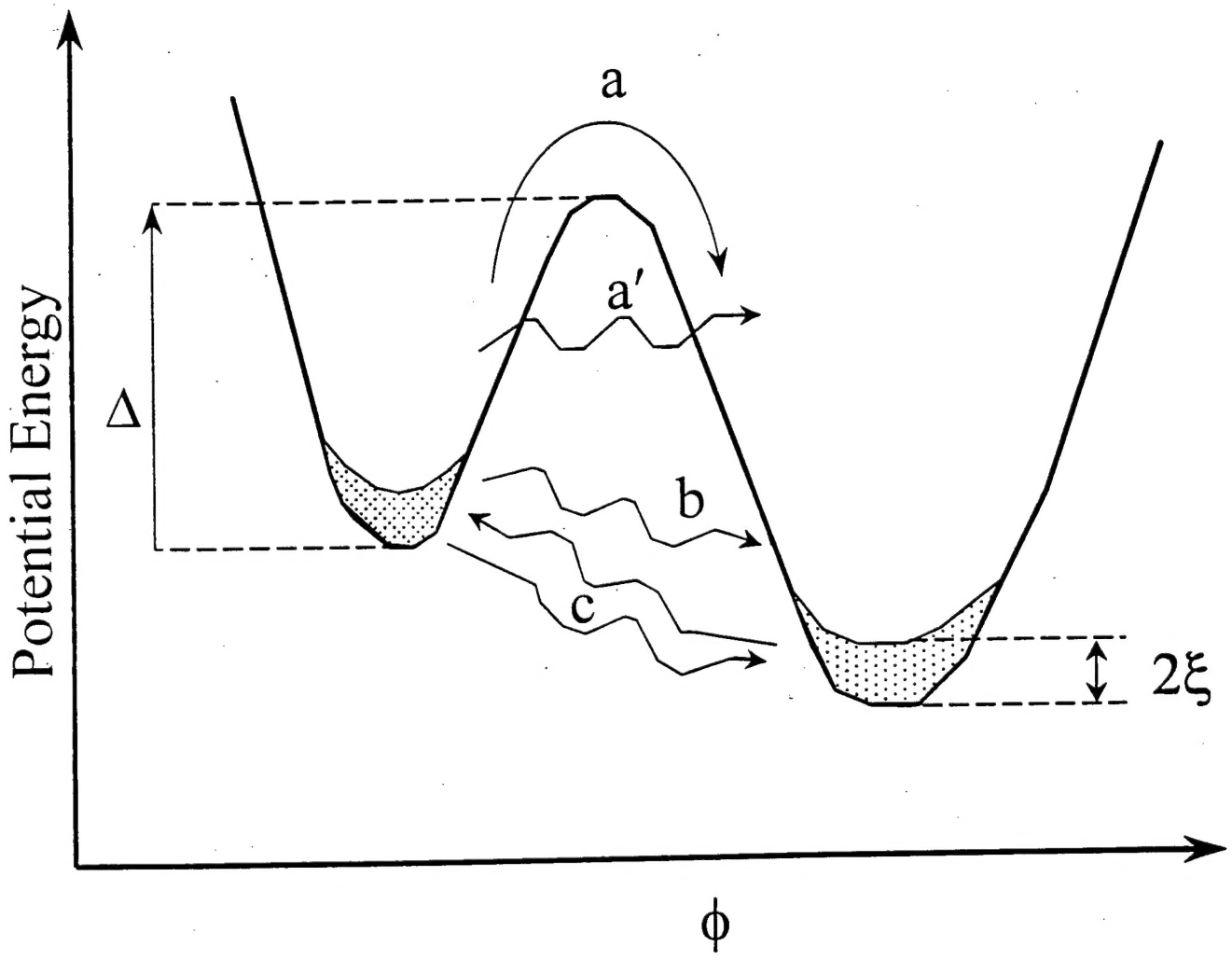
Potential Energy
a
a′
Δ
b
c
2ξ
ϕ

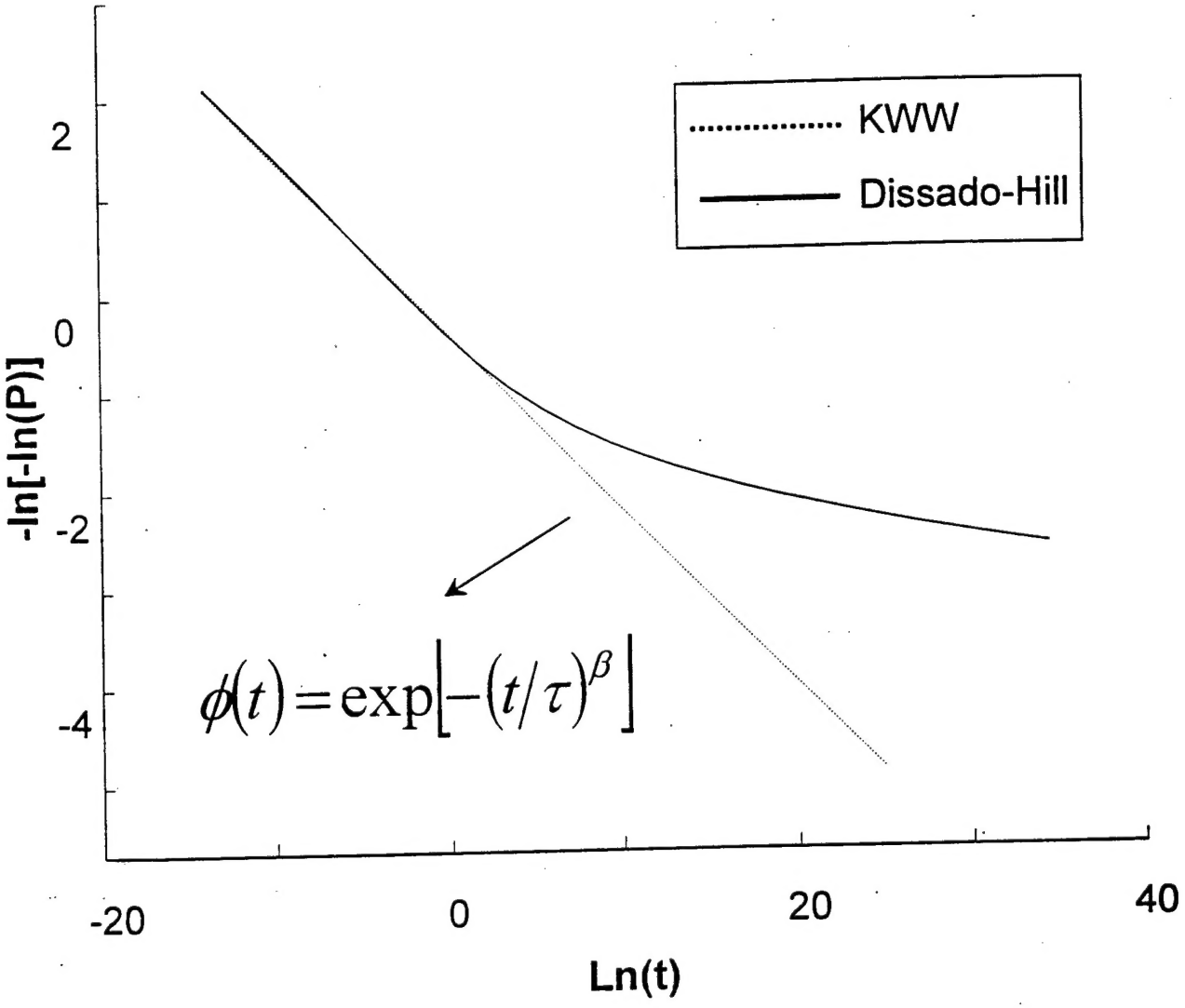
KWW
Dissado-Hill
2
0
-2
-4
-ln[-ln(P)]
-20
0
20
40
Ln(t)
$\phi(t) = \exp\left[-(t/\tau)^{\beta}\right]$

Specific Volume V
Temperature T
$q \to 0$
α_G
$q_1 > q_2$
q_2
q_1
α_L
T_2 T_{g2} T_{g1} T_f